# Evaluating earthquake-induced rockfall hazard by investigating past rockfall events: the case of Qiryat-Shemona adjacent to the Dead Sea Transform, northern Israel

## Authors' Comments for Reviewer #1

Mor Kanari[1], Oded Katz[2], Ram Weinberger[2], Naomi Porat[2], Shmuel Marco[3]

[1]Department of Marine Geology and Geophysics, Israel Oceanographic and Limnological Research, Haifa 31080, Israel
[2]Geological Survey of Israel, 30 Malkhe Israel St. Jerusalem 95501, Israel
[3]Department of Geophysics, Tel-Aviv University, Tel-Aviv 69978, Israel

*Correspondence to*: Mor Kanari (mor.kanari@ocean.org.il)

**General:** Reviewer #1's comments were of great contribution to the manuscript, addressing these issues and revising the text and figures accordingly has benefitted the manuscript and helped to obtain better supported arguments for our discussion and conclusions, and improve the way we present our results and address critical issues in the discussion.

We thank the reviewer very much for taking the time to raise questions and make suggestions that improved the manuscript significantly.

All of the reviewer's comments were addressed or answered and changed in the manuscript. Our reply comments are brought here in a numbered item-list detailing each of the comments with the explanations and actions we introduced accordingly.

** **Important Note – OSL dating revision**: additional to reviewer comments, which were all answered as detailed below, we have also *made more OSL measurements per sample* since they were originally done several years ago and since then the protocols have been updated and augmented. In this version we present the newly updated OSL results, which give better age constrains with significantly smaller error bars and hence more accurate and reliable ages. The relevant figures (Fig 10 and Fig 11), tables (Table 3 and Table 4) and text (Section 4.3 – results and Section 5.4 - discussion) were revised accordingly.

(1) **Comments from Referee:** Section 3.1. Authors should provide some information about the block size; this should explain why in the subsequent sections they use only selected values of the block sizes.

Author's response: This was missing here although detailed later in the text of the results. Details of the field mapped block sizes were added to section 3.1 and its paragraph was revised. The use of selected block values for the simulation was added to the next section (3.2) to be presented before the calibration methodology.

Author's changes in manuscript: section 3.1 revised and added the following: "76 blocks were mapped and measured in the field with volumes varying between 1.0 $m^3$-125.0 $m^3$."

Section 3.2 was added the following: "The simulated block volumes were binned into size scales of 1, 10, 50, 100, 125 $m^3$, with corresponding block diameters of 1.3, 2.7, 4.6, 5.8 and 6.2 m, respectively (assuming spherical block geometry)."

(2) **Comments from Referee:** Section 3.3. The calibration method is not clear, since two out four pink lines are out of the field mapping (green polygon in Fig. 3) and it seems that only one of the lines intersects a relatively boulder-dense area. Please, explain better this point and give the number of the field-mapped rock-blocks ("high" is too generic).

Author's response: The text was revised accordingly to better explain the calibration profiles locations.

Author's changes in manuscript: This paragraph in section 3.3 now reads as follows:

"In the current work, CRSP calibration using back-analysis was performed along four slopes (pink lines in Fig. 3) located at the N and S parts of the prominent Ein-El-Assad source outcrop, where a relatively high number of field mapped (50 blocks out of 76) and aerial photo mapped rock-blocks (65 blocks out of 200) were observed."

(3) **Comments from Referee:** Line 31, page 4, a different letter for the velocity (e.g. u) should be used, since V is the block volume.

Author's response: This is a good point. All 'Vx'mentioned in the section were replaced to 'Ux'

Author's changes in manuscript: All 'Vx'mentioned in the section were replaced to 'Ux'.

(4) **Comments from Referee:** A simulation is supposed to output a mean value and an uncertainty, but the reported results of the sensitivity analysis are sharp numbers. Could the authors give an uncertainty on these numbers?

Author's response: The optimal Rn=0.22 value was extracted using a regression curve from the $\Delta MD$ values (difference between observed and simulated maximum travel distance) resulting from testing end members 0.12, 0.2, 0.25. when fitted a regression with minimum difference between simulated and observed maximum travel distances the regression yielded a minimum of 0 difference at 0.22. an explanation for this and an estimation for the change in travel distance per 0.01 change in Rn was revised in the text.

Author's changes in manuscript: the text in section 3.3 was revised accordingly and now reads as follows:

"An exponential regression curve was fitted for the above $R_n$ values (0.12, 0.2, 0.25) vs their corresponding $\Delta MD$ values (-90, -30, +160 m), which yielded $\Delta MD$ = 0 m (minimum difference between observed and simulated maximum travel distance) at $R_n$ = 0.22. Thus, calibration was determined optimal for $R_n$ = 0.22. We estimate that 0.01 change in Rn will yield 15-30m change in maximum travel distance. Calibration profiles are 450-750 m, yielding 2%-3% variability for 0.01 change in $R_n$."

(5) **Comments from Referee:** Is the surface roughness S a dimensionless quantity in the CRSP algorithm? If not, please add the proper measurement unit (feet, meters?.

Author's response: Surface roughness was measured in the field according to the CRSP program manual. It is given in meters but varies according to the radius of the simulated block. Hence an S value per simulated block diameter needs to be measured in the field and used in the software. S values were revised to have meter units in the text.

Author's changes in manuscript: text revised accordingly as follows:

"… using the above detailed best-fit values $R_n$=0.22; $R_t$=0.70 and the field-measured surface roughness S values S=0.1, 0.3, 0.4 m for block diameters D=1.3, 2.7, 4.6 m respectively, and S=0.5 m for D=5.8 and 6.2 m (all S values were measured in the field per block diameter according to CRSP software manual)."

(6) **Comments from Referee:** Lines 6 to 8, page 5. This statement is not clear, please rephrase it.

Author's response: paragraph was modified to better explain and detail the calibration process.

Author's changes in manuscript: lines 6-8 were revised accordingly and now read:

"$R_t$ value was determined to 0.70 following our initial calibration value, which is also recommended by Jones et al (2000) for firm soil slopes. To validate these coefficients, further simulation runs along the four calibration profiles were performed for all block sizes (D=1.3–6.2 m), using the above detailed best-fit values $R_n$=0.22; $R_t$=0.70 and the field-measured roughness S values: S=0.1, 0.3, 0.4 for block diameters D=1.3, 2.7, 4.6 m respectively, and 0.5 for D=5.8 and 6.2 m (all S values were

measured in the field per block diameter). All slope cells were given the same values to maintain model simplicity. The travel distances of simulation results were compared with the observed travel distances (from field mapping and aerial photo mapping). The fit between observation and simulation is plotted in Fig. 5."

(7) + (8) **Comments from Referee:** Section 4.1. The scaling exponent of the probability density function is -1.17. How much are the authors confident on the second decimal number? Could you give an estimation of the uncertainty on this number? If not, I would give -1.2 as a likely value.

Lines 23 to 28, page 6, need to be better explained. How does Eq. (2) relate to Eq. (3)? In Eq. (2), the cumulative probability for blocks with diameter less or equal to D is the sum from Vmin to VD (the integral for very small bins) of the probabilities calculated for each bin. Applying the relationship between volume V and diameter D for a sphere (V = 4/3Â°upiÂ°u(Dˆ3)/8 ) in Eq. (2) does not yield the expression shown in Eq. (3). Could you explain the difference? As in the previous comment, how much are the authors confident on the decimal values in Eq. (3)?.

Author's response: The reviewer suggestion to round the power law to -1.2 is correct. The -1.17 It is yielded from the regression but the $R^2$ is not very high (0.72). The text was revised to detail the calculated -1.17 power and suggest to round it to -1.2.

The discrepancy between Eq 2 (all blocks 1-125 $m^3$) and Eq. 3 (only block diameters 2.7-6.2 for volumes 10-125 $m^3$) is because eq 3 is used for correlating our actual volumes (diameters) of the simulated larger size blocks in which we are interested for the hazard estimation. The smaller scale blocks (1 $m^3$) are of less interest for hazard estimation as we focus on the larger blocks as potential worse-case hazard in our simulations. We later use Eq 3 for prediction of probability for occurrence of blocks at sizes up to 10-125 $m^3$ (D=2.7-6.2 m) for hazard calculations.

Author's changes in manuscript: The text in section 4.1 regrading these two comments was revised accordingly and now reads as follows:

"Our results show that the volume of the individual rock blocks from the studied area exhibits a distinct negative power law behavior, with a scaling exponent of the right tail of $\alpha$ = -1.17 ($R^2$ = 0.72; Fig. 6). This conforms to what was found by others who examined natural rockfalls with observed $\alpha$ ranging: -1.07 - -1.4, e.g., Guzzetti et al. (2003) Malamud et al. (2004) Brunetti et al. (2009). The scaling exponent is also similar to the value $\alpha$ = -1.13 obtained experimentally by Katz and Aharonov (2006), while Katz et al. (2011) found a larger scaling exponent, $\alpha$ = -1.8. Since our data yield a moderate inner consistency $R^2$=0.72 we round the power to -1.2 (instead of -1.17). In accordance, the probability density function (PDF) for rockfall volume (*p)* may be presented as a power law of the form (Dussauge-Peisser et al., 2002; Dussauge et al., 2003; Guzzetti et al., 2003; Malamud et al., 2004) Eq. (2), where *V* is the given block volume in $m^3$:

$$p = 0.4V^{-1.2} \qquad (2)$$

To simplify the hazard evaluation and relate to the more prominent hazard which larger block sizes impose (thus removing the 1 $m^3$ smaller blocks from the simulation runs) the block volumes were binned into size scales of 10, 50, 100, 125 $m^3$, with corresponding block diameters of 2.7, 4.6, 5.8 and 6.2 m respectively (assuming spherical block geometry). Field mapped cumulative frequencies were used to derive cumulative probabilities for each block size (Table 1). The probability values per block diameter (Table 1) were fitted a regression curve in Excel ($R^2$ = 0.97), yielding the probability ($p_D$) for a block of given diameter (*D*) or smaller following Eq. (3):

$$pD = 0.412Ln(D) + 0.262 \qquad (3)$$

The cumulative probability calculated from Eq. (3) per block diameter differs from the cumulative probability calculated in Eq. (2) per its matching block volume because of the differences in data-sets and usage of the two equations: Eq. (2) power-law details our full field-observed data of block sizes and is used to characterize the dataset and compare it to other block

catalogs in other studies. While Eq. (3) yields a simulation-specific empirical prediction for probability of occurrence for the larger block diameters (D>=2.7 m; V>=10 $m^3$), which were actually used later in the CRSP simulations for hazard analysis."

(9) **Comments from Referee:** Section 4.2.1. Could authors give a definition of the profile cell? What is the size of it? Fig. 7 is potentially interesting, but I'm not sure to have fully understood it. The number of profiles shown on the horizontal axis is 30, while in the Figure caption is 25. The vertical axis title should be better placed along the graduated curved axis. Grey circles are defined as "other cells". Could the author explain better what these other cells represent?

Author's response: An explanation for slope cell in CRSP was added in section 3.2 in the methods. Figure 7 has been modified (profile axis numbers fixed) and now includes also an illustration of the CRSP model slope cells, x% stop angles and the stop swath. Additional explanation of the figure was added to the figure caption and is referred to in the text in section 4.2.1

Author's changes in manuscript:

* Methods section '3.2 rockfall simulations' was added the following explanation about the slope cell: "The slope surface in CRSP is divided into slope cells, which boundaries are defined where the slope angle changes, or where the slope roughness changes (Jones et al., 2000)."

* Section 4.2.1 was added the following reference to figure 7: "Further details and illustration for slope cells and stop angles are given in Fig 7."

* Figure 7 revised caption now reads as follows:

**"(a)** Schematic illustration of the CRSP modelled slope cells and explanation of the terms 'x% slope angle' (e.g. 50% stop angle is the angle of the slope cell where 50% of the blocks stop) and 'stop swath' (the farthest distance along the last cell where 100% of the blocks stop)**. (b)** Slope gradients of slope cells and gradients at stop angles. Tangential axes (X and Y axes) denote simulated profile numbers 1 to 25. Radial axis denotes the slope angles. Gradients for all cells per profile are plotted on an arc between 0 and 90 degrees: Red circles are 100% stop angles (slope angle of the profile cell at which cumulated 100% of simulated blocks stop); blue triangles are 50% stop angles; gray circles are all other cells in the profile. For example: the cells along profile 16 have slope angles that vary between 8°-36°; the 100% stop angle is 11° (red circle) and the 50% stop angle is 8° (blue triangle). The red line represents the mean of all 100% stop angles for all profiles at 7.7° and the thick black lines represent its SD of 2.3°."

(10) **Comments from Referee:** Line 11, page 7, how do you calculate the range of variation 3_-12_ from a mean of 7.7_ and a SD of 2.3_?

Author's response: the variation presented is for the whole range of stop angles. the mean and 1sigma SD (2.3) yield a 6.4-10 deg. Text revised accordingly.

Author's changes in manuscript: revised text now reads as follows:

"100% stop angles for all profiles (red circles in Fig. 7) vary between 3°-12° with a mean of 7.7° and *SD* = 2.3° (1σ=6.4°-10.0°); 50% stop angles (blue triangles) vary between 3.2°-25.8° with a mean of 10° and *SD* = 5.3° (1σ=4.7°-15.3°). All other cell slope angles in all profiles (gray circles) vary widely between 7°-88° with a mean of 29.4° with *SD* = 17° (1σ=12.4°-46.4°)".

(11) **Comments from Referee:** Section 5.1. The sentence: "Thus, rainstorms are ruled out as a favorable triggering mechanism" should be smoothed since it is supported by a very poor statistics, i.e. only two seasons.

Author's response: the statistical data was re-phrased, and more importantly – a comparison of another rockfall study in Yosemite in which 27% (>100) of reported rockfall events in 150 years were triggered by rainstorms is brought as a counter example to support our suggestion that rainstorms are not a favorable trigger, with no reports of rockfalls for the past 74 years at all, in spite of heavy rainstorms in the study area were reported. Additionally – we added reference to the current

year's harsh winter (2019), which is of decades scale extremity in its winter storms, as an example where no evidence for rockfall were observed.

Author's changes in manuscript: The text was revised and now reads as follows:.

"The correlation of rockfall events to historical extreme rainstorm events is limited due to the lack of long enough historical rainstorm record. However, in the 74 years of documented climatic history for the studied area (measurements at the 5 km away Kfar-Blum station since 1944; IMS, 2007) no significant rock-mass movements and rockfalls were reported in the study area. Thus period includes the extremely rainy winters of 1968/69 and 1991/92, in which annual precipitation in northern Israel was double than the mean annual precipitation (IMS, 2007). Furthermore, the winter of 2018-2019 (during which the current study is being prepared for publication) breaks a five-year drought that was the worst Israel has experienced in decades (Time of Israel, 2019), with massive floods, snowfall, overnight freeze and rainstorms in Northern Israel, including in the study area. The authors of the current study received 1st-hand personal correspondence (photos, videos and descriptions) from hikers on the studied slope, which observed some dismantling of rock blocks in their location during one of the large rainstorms in Jan-2019. Yet no rockfall events were documented in the study area during this extreme winter season. Contrastingly, Wieczorek and Jäger (1996) reported that out of 395 documented rockfall events in the Yosemite Valley which occurred between 1851 and 1992, the most dominant recognized trigger for slope movement was precipitation (27% of reported cases), and point out the influence of climatic triggering of rockfall. Based on this large difference of observations, we suggest that rainstorms may not provide a major triggering mechanism for rockfalls in our study area".

(12) **Comments from Referee:** In Sect. 5.2 the correlation observed between rockfall events and earthquakes is investigated only for the largest blocks, therefore rainstorms cannot be ruled out for small-size blocks.

Author's response: That is true. The prerequisite for OSL dating was using large blocks, hence any correlation to earthquakes is for the larger blocks (V>= 8 $m^3$ / D>=2.5 m). However – the rockfall simulation blocks used for hazard analysis also answer to these volumes (smallest simulated blocks were 10 $m^3$ or D=2.7 m). Additionally, since the larger blocks pose greater hazards in terms of destructive potential, we aimed for analysis of the larger blocks for relevance to the rockfall hazard estimation. The previous section 5.1 was revised according to reviewer's notes and now discusses the rainstorms as possible trigger (and suggests they are not a favorable one).

Author's changes in manuscript: At the beginning of section 5.2 the following was added: "The following discussion relates to blocks of sizes equal or larger than 8 $m^3$ (D>2.5 m) as the OSL dated blocks were of sizes 8-80 $m^3$. These volumes fit the CRSP simulation analyses of all blocks in the study, as the smallest simulated block for the hazard estimation was 10 $m^3$ (D=2.7 m)."

(13) **Comments from Referee:** Section 5.3.2. This subsection, which is the main outcome of the manuscript requires to be rewritten in a more understandable form. The hazard contains usually three terms: one is a time-dependent term, one is size dependent and another one is the susceptibility. Starting from this definition the author should describe each term on the base of the results described in the previous sections of the manuscript.

Author's response: Thank you for this remark. The text in section 5.3.2 was completely revised following the reviewer's recommendation. The section is now numbered "5.4".

Author's changes in manuscript: section 5.4 (previously 5.3.2) now reads as follows:

"We discuss the hazard probability by addressing three terms: time dependency, size dependency and susceptibility.

**Time dependency:** we derive the recurrence time for rockfalls in the study area by correlating OSL dating of rockfall events to past earthquakes, as detailed above. Thus, we can calculate the probability of a rockfall occurrence $P_{EQ}$ in the next 50 years, assuming earthquake magnitude Mw = 6 as the threshold for rockfall: $P_{EQ}$ = 50/550 = ~0.09 or 9%. We do not present

a time-dependent earthquake recurrence interval calculation because the time passed since the last large earthquake is not well constrained.

**Size dependency**: Based on the field mapping of block sizes and the expected block sizes which correspond both to the sizes of OSL dated blocks and the CRSP simulation block diameters (Table 1; Fig. 3), the probability of a given block size or smaller is predicted by Eq. (3). Considering the time dependent probability and the probabilities for given block sizes detailed above, the probability for rockfall hazard per specific block size ($H_R$) may be predicted as Eq. (5):

$$H_R = (1 - P_D) \cdot P_{EQ} \qquad (5)$$

where $P_D$ is the cumulative probability per block diameter D (Table 1) and $P_{EQ}$ is the rockfall occurrence probability calculated above to be 9%. Accordingly, predicted $H_R$ for the next 50 years for block diameters D between 2.7 - 6.2 m is ~3% and for larger blocks, D between 4.6 - 6.2 m is ~1%.

**Susceptibility:** As presented in Figures 8-9, the urban area and the area of open slopes above it subjected to rockfall hazard extends to about 1.55 km$^2$. We conclude that this area has a probability $H_R$ of ~1% - 3% for impact by rockfall in the next 50 years.**"**

(14) **Comments from Referee:** Technical corrections See attached PDF file.

Author's response: **All reviewer's technical corrections were implemented in the text accordingly** (including grammar, revision of paragraphs for details, clarifications or better English).

Author's changes in manuscript: **We implemented many technical changes throughout the text and figures following all reviewer's comments**.

Only in one place the suggested technical correction/notes were not implemented, for which explanation is given here as follows: Page 30 – reviewer comment: The figure could be more readable if the triangles and the numbers were only on the yellow line.

Author's response: The triangles and numbers appear both on the yellow line and the red dashed line in ptofiles 8-9-10-11-12-13-14-16 because these are the profiles where block impact is predicted to hit town border. The yellow line is the predicted stop line and the red dashed line is where the blocks are predicted to hit town premises before stopping. For each of these profiles there is double nomenclature: (1) at impact point where kinetic analysis is performed: a triangle marking the location of impact and a 'sword'profile number; (2) at predicted stop point: a triangle marking stop location and a regular profile number. Thanks for helping to clarify – we distinguished the impact / stop locations in different colors.

Author's changes in manuscript: in Fig 9: Town border impact locations were marked in orange triangles, while simulated stop locations were marked in yellow triangles for better clarity. The Figure caption was revised accordingly.

**Revised figures 4, 7, 9, 10, 11 appear in the next pages**

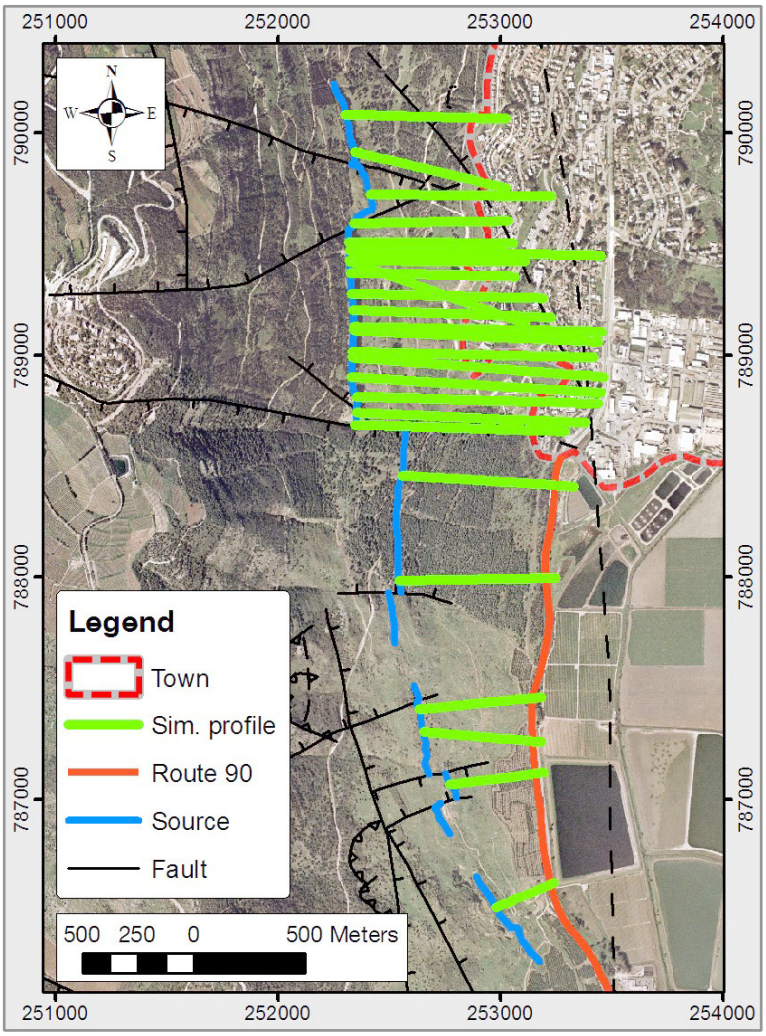


Fig.4 – revision included brightening the background for better clarity of the faults (marked in black lines).

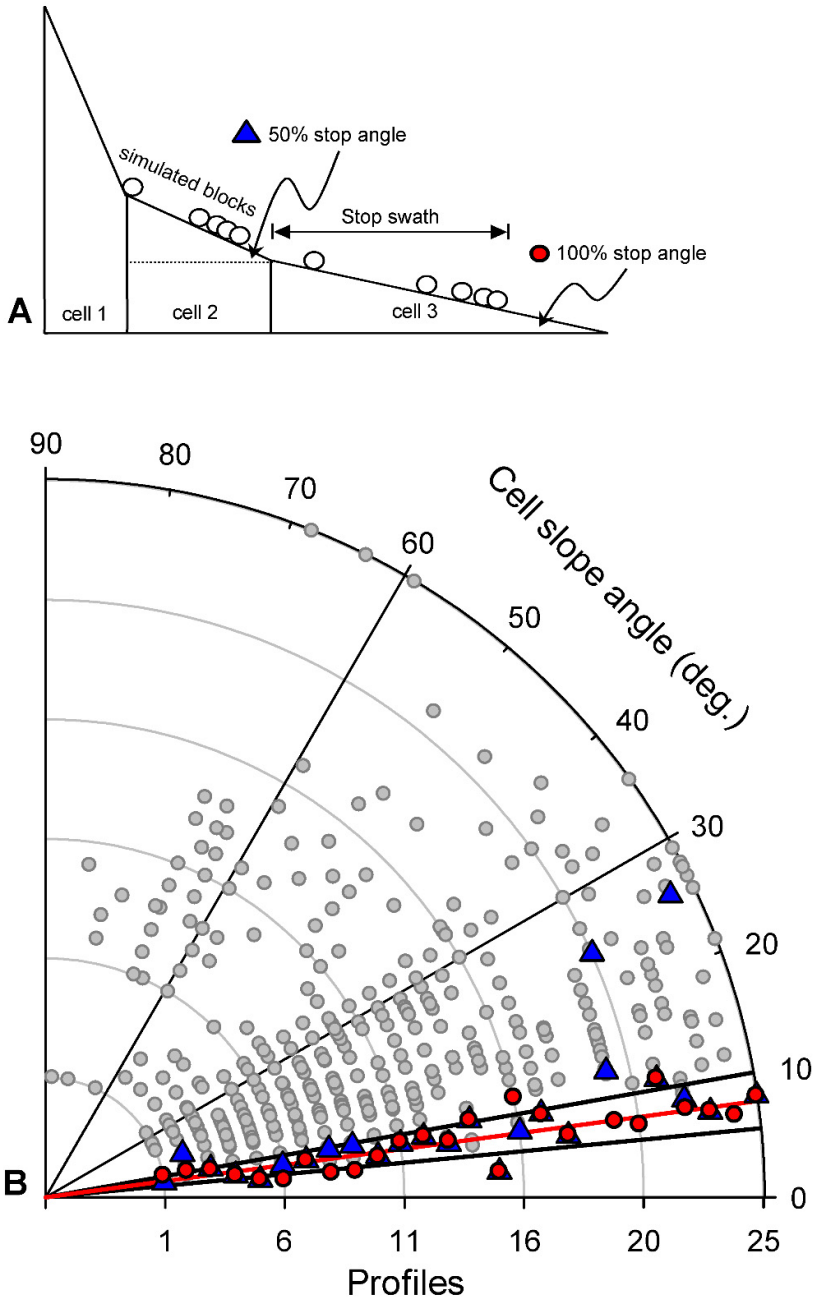


Fig 7. Revised for better clarity of the axes and their representation, and added a top panel which gives an illustration of the terms used in the simulation discussion (profile cells, stop angles, stop swath etc.)

5

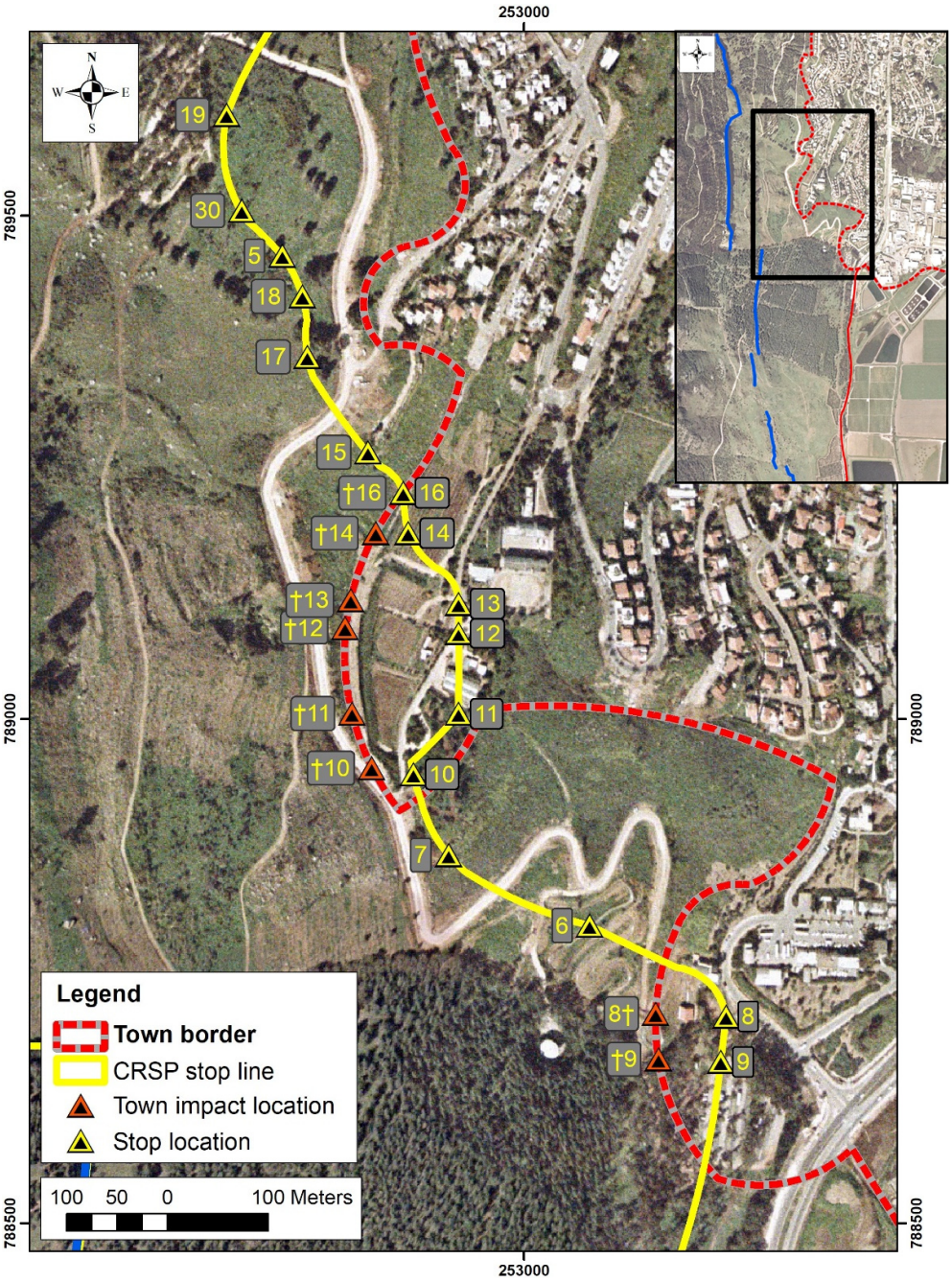


Fig 9. Revised for clarity: Town border impact locations were marked in orange triangles, while simulated stop locations were marked in yellow triangles for better clarity, figure caption revised accordingly.

5

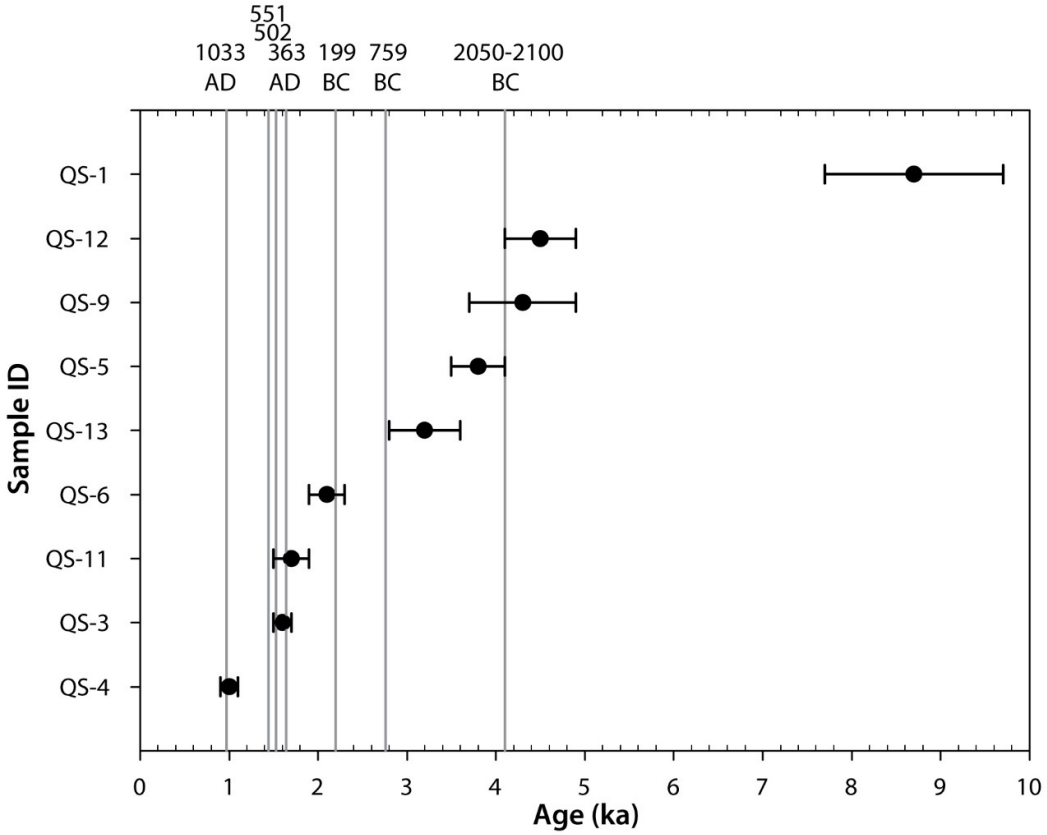


Fig. 10 – revised OSL age determination following repeated lab results.

5

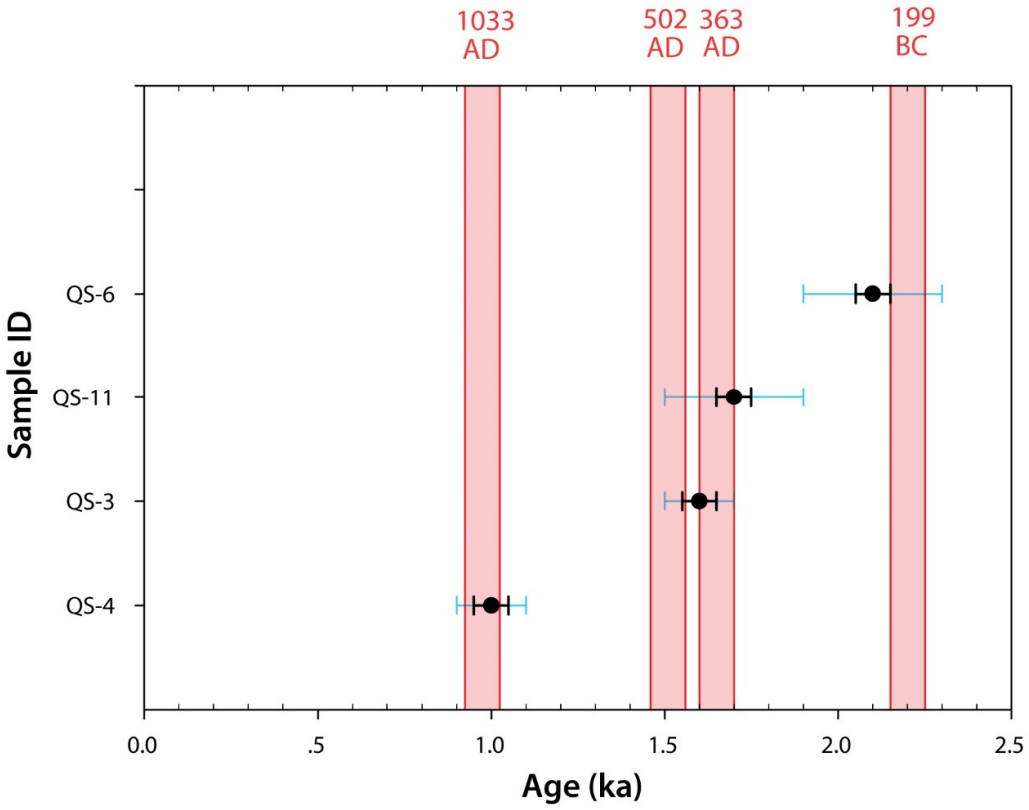


Fig. 11 – revised OSL age clustering analysis following repeated OSL dating lab results.

5

# Evaluating earthquake-induced rockfall hazard by investigating past rockfall events: the case of Qiryat-Shemona adjacent to the Dead Sea Transform, northern Israel

## Authors' Comments for reviewer #2

Mor Kanari[1], Oded Katz[2], Ram Weinberger[2], Naomi Porat[2], Shmuel Marco[3]

[1]Department of Marine Geology and Geophysics, Israel Oceanographic and Limnological Research, Haifa 31080, Israel
[2]Geological Survey of Israel, 32 Yeshayahu Leibowitz St. Jerusalem 9371234, Israel
[3]Department of Geophysics, Tel-Aviv University, Tel-Aviv 69978, Israel

*Correspondence to*: Mor Kanari (mor.kanari@ocean.org.il)

**General:** The comments and suggestions made by Reviewer #2 have a significant and important contribution to the manuscript quality and readability. The revisions introduced to the text following the review improved the manuscript and helped to consolidate its structure and make it more clear for reading. Following the reviewer's notes we extensively improved the abstract and introduction parts, thus aiding to present the essence of the study, as well as its importance and its relevance to other studies.

* All of the reviewer's comments were addressed or answered and changed in the manuscript.

* Our reply comments are hereby brought in this SUPPLEMENT PDF file in a numbered item list detailing each of the comments with the explanations and revisions-actions we introduced to the manuscript accordingly.

We thank the reviewer very much for taking the time to raise questions and make suggestions that improved the manuscript significantly.

(1) **Comments from Referee:** Abstract - I suggest rewriting the abstract because it is mixed up. It lacks a framework. Aims and methods are not clearly defined.

Author's response: The abstract was revised according to the reviewer suggestions. it is now more complete and details the framework to detail the study.

Author's changes in manuscript: abstract was revised and reads as follows:

"We address an approach for rockfall hazard evaluation where the study area resides below a cliff in an a priori exposure to rockfall hazard, but no historical documentation of rockfall events is available and hence, important rockfall hazard parameters like triggering mechanism and recurrence interval are unknown.

We study the rockfall hazard for the town of Qiryat-Shemona, northern Israel, situated alongside the Dead Sea Transform, at the foot of the Ramim escarpment. Numerous boulders are scattered on the slopes above the town, while pre-town historical aerial photos reveal that boulders had reached location that are now town premises. We use field-observations and Optically Stimulated Luminescence dating of past rockfall events combined with computer modeling to evaluate the rockfall hazard. For the analysis, we first mapped the rockfalls source and final downslope stop-sites and compiled the boulder size distribution. We then simulated the possible rockfall trajectories using the field observed data to calibrate the simulation software by comparing simulated and mapped boulders stop-sites along selected slopes, while adjusting model input parameters for best fit. The analysis reveales areas of high rockfall hazard at the south-western quarters of the town and also indicates that in the studied slopes, falling blocks would stop where the slope angle decreases below 5°-10°. Age determination suggests that the rockfalls were triggered by large (M >6) historical earthquakes. Nevertheless, not all large

historical earthquakes triggered rockfalls. Considering the size distribution of the past rockfalls in the study area and the recurrence time of large earthquakes in the region, we estimate a probability of less than 5% to be affected by a destructive rockfall within a 50-year time-window.

We suggest here a comprehensive method to evaluate rockfall hazard where only past rockfall evidence exists in the field. We show the importance of integrating spatial and temporal field-observations to assess the extent of rockfall hazard, the potential block size-distribution, and the rockfall recurrence interval."

(2) **Comments from Referee:** Introduction - It is too brief. I suggest rewriting this section in order to enlarge the scientific literature discussion, for better insert the proposed study in the methodological state of the art.
Moreover, the authors jump from the presentation of the background to presenting their work without any connection.

Author's response: Good point. The first part of the introduction was revised and now has references to previous works dealing with rockfall trigger mechanisms and rockfall dating and hazard estimations.

Author's changes in manuscript: Tthe introduction was revised according to reviewer suggestions now reads as follows:

"Rockfalls are a type of fast mass movement process common in mountainous areas worldwide (Dorren, 2003; Flageollet and Weber, 1996; Mackey and Quigley, 2014; Pellicani et al., 2016; Strunden et al., 2015; Whalley, 1984). In this process, a fragment of rock is detached from a rocky mass along a pre-existing discontinuity (e.g., bedding, fractures) slides, topples or falls along a vertical or nearly vertical cliff. Individual fragments travel downslope by bouncing and flying or by rolling on talus or debris slopes (Crosta and Agliardi, 2004; Cruden and Varnes, 1996; Varnes, 1978; Whalley, 1984, Wei et al., 2014). The rock fragments travel at speeds of a few to tens meters per second, and range in volume up to thousands of cubic meters. Different mechanisms are known to trigger rockfalls: earthquakes (Kobayashi et al., 1990; Vidrih et al., 2001), rainfall and freeze-and-thaw cycles (Wieczorek and Jäger, 1996; D'amato et al., 2016). Due to their high mobility, and despite their sometimes small size, rockfalls are particularly destructive mass movements, and in several areas they represent a primary cause of landslide fatalities (Evans and Hungr, 1993; Evans, 1997; Guzzetti, 2000; Keefer, 2002; Guzzetti et al., 2003; Guzzetti et al., 2005; Badoux et al., 2016). In mountainous areas human life and property are subject to rockfall hazard (Crosta and Agliardi, 2004) and efforts are made to mitigate the hazard. Mitigation measures for rockfall damage are primary based on hazard assessment, which integrates all available data to map and scale the hazard (e.g. Guzzetti et al., 2003). The spatial extent of the hazard in many cases can be resolved using field observations of documented historical rockfalls (Wieczorek and Jäger, 1996) and computer modeled trajectories (Dorren, 2003 and references therein). The temporal aspect of hazard and the triggering mechanism usually rely on historical reports, but rarely on direct dating of past rockfall events (e.g. De Biagi et al., 2017; Kanari, 2008; Rinat et al., 2014). However, hazard estimation where no historical documentation of past rockfalls exists (hence no documentation of neither the spatial and temporal extents), nor any knowledge of the triggering mechanism, such as the case presented here, is rare or missing in literature.

The current study evaluates the rockfall hazard for the town of Qiryat-Shemona (northern Israel), by (a) studying the extent and nature of past rockfall events using field observation; (b) Constraining the date of the rockfall events and their reoccurrence interval using optically stimulated luminescence (OSL) dating (Wintle, 2008). The possible temporal relation to known historical earthquakes, which might serve as a trigger, is also studied; (c) computer-modeling the most probable down-slope rockfall trajectories which outline the hazard-prone area. Particular attention is given to the calibration of the computer modeling using mapping of past rockfall events and extracting geometrical and mechanical parameters needed for the simulations from the field observations. This study presents a methodology for rockfall hazard estimation where field evidence for past rockfalls are observed in the town vicinity, but the triggering mechanism, the timing of past rockfall events and recurrence intervals are entirely unknown."

(3) **Comments from Referee:** Methods – I suggest inserting, especially for paragraph 3.1, literature references about the methodology based on the correlation block distribution-dimension

Author's response: References for several of block inventory/dimension and distribuiotm were added to paragraph 3.1. they are also later discussed in the block size distribution results in section 4.1 in the original manuscript.

Author's changes in manuscript: Section 3.1 was revised according to reviewer suggestion and now begins with the following:

"In a given site, the size distribution of boulders resulting from past local rockfalls (recent or historical) is the best database for assessing predicted rockfall block size. Thus mapping the blocks is crucial for hazard analysis, as suggested by previous studies that required estimations or measurements of the number of blocks and their volumes (Brunetti et al., 2009, Dussauge-Peisser et al., 2002; Dussauge et al., 2003; Guzzetti et al., 2003; Malamud et al., 2004; Katz and Aharonov, 2006; Katz et al., 2011)."

(4) **Comments from Referee:** Results and discussion – These sections are subdivided into too subparagraphs. The readability and understanding of the research outputs could be compromised and made confused by the organization of these sections. I suggest to reorganized these sections.

Author's response: Regarding the **Results**: we have results of many kinds: field mapped blocks, software simulations of several aspects (hazard area mapping, travel distances, kinetic energy calculation, slope angles) and OSL dating of rockfalls. We find it necessary to split the paragraphs in the software simulation results for better presentation of the many types of results we discuss in the study. Therefore we prefer to keep the results in their original order with sub-headings (4.2.1 etc.) for the different analyses we made for the simulation results.

Regarding the **Discussion:** we agree with the reviewer that there is too many sub-headings and they were simplified to single-level headings in the manuscript.

Author's changes in manuscript: Discussion sections were numbered 5.1…5.4 and sub-section headers were removed (e.g. 5.3.1 etc.).

(5) **Comments from Referee:** **Technical corrections** Pag. 1 line 26: better "a rocky mass" than "the bedrock". Pag. 2 line 23: replace the colon with a dot. Pag. 3 lines 23-24: better "geometry and properties of in-situ rocky mass and of detached blocks". Pag. 3 line 27: please put the references into parentheses. Pag. 3 line 29: replace the colon with a dot. Pag. 4 line 10: how were the source areas identified?

Author's response: **All of the technical corrections suggested by the reviewer were implemented in the text** (except for one colon that we could not identify in the text in page 3 line 29).

Author's changes in manuscript: Text revised according to reviewer suggestions. Regarding the identification of the source areas – the following clarification was added to the text in the 'study area' description:

"Colluvium and rock-mass movement deposits were mapped on the slopes near Qiryat-Shemona (Shtober-Zisu, 2006, Sneh and Weinberger, 2003a), *identifying the blocks on the slope as originating from the Ein-El-Assad formation*."

**Track Changes Manuscript**

**In the next pages is the revised version of the manuscript in 'Track Changes' to demonstrate the changes to the original manuscript following the reviewers' notes.**

# Evaluating earthquake-induced rockfall hazard by investigating past rockfall events: the case of Qiryat-Shemona adjacent to the Dead Sea Transform, northern Israel

Mor Kanari[1], Oded Katz[2], Ram Weinberger[2], Naomi Porat[2], Shmuel Marco[3]

[1]Department of Marine Geology and Geophysics, Israel Oceanographic and Limnological Research, Haifa 31080, Israel
[2]Geological Survey of Israel, ~~30 Malkhe Israel~~32 Yeshayahu Leibowitz St. Jerusalem ~~95501,~~ 9371234, Israel
[3]Department of Geophysics, Tel-Aviv University, Tel-Aviv 69978, Israel

*Correspondence to*: Mor Kanari (mor.kanari@ocean.org.il)

**Abstract.** ~~We evaluate~~

We address an approach for rockfall hazard evaluation where the study area resides below a cliff in an a priori exposure to rockfall hazard, but no historical documentation of rockfall events is available and hence, important rockfall hazard parameters like triggering mechanism and recurrence interval are unknown.

We study the rockfall hazard for the town of Qiryat-Shemona, northern Israel, situated alongside the Dead Sea Transform, at the foot of the Ramim escarpment. ~~Boulders of 1 m$^3$ to 125 m$^3$~~ Numerous boulders are scattered on the ~~slopes~~slopes above the town, while pre-town historical aerial photos reveal that ~~before town establishment, numerous~~ boulders had reached ~~the~~location that are now town premises. We use field-observations and Optically Stimulated Luminescence dating of past rockfall events combined with computer modeling to evaluate the rockfall hazard. For the ~~hazard~~ analysis, we first mapped the rockfalls~~, their~~ source and ~~their~~final downslope ~~final~~ stop-sites~~,~~ and compiled the boulder size distribution. We then simulated the ~~probable future~~possible rockfall trajectories using the field observed data to calibrate the simulation software by comparing simulated ~~vs~~and mapped boulders stop-sites along selected slopes, while adjusting model input parameters for best fit. The analysis ~~identified~~reveals areas of high rockfall hazard at the south-western quarters of the town and also indicates that in the studied slopes, falling blocks would stop ~~after several tens of meters~~ where the slope angle ~~is~~decreases below 5°-10°.

~~OSL age~~Age determination ~~of several past rockfall events in the study area~~ suggests that ~~these~~the rockfalls were triggered by large (M >6) historical earthquakes. Nevertheless, not all large historical earthquakes triggered rockfalls. ~~Simulations show that downslope reach of the blocks is not significantly affected by the magnitude of seismic acceleration.~~ Considering the size distribution of the past rockfalls in the study area and the ~~reoccurrence~~recurrence time of large earthquakes in the region, ~~the~~ we estimate a probability of less than 5% to be affected by a destructive rockfall within a 50-~~-~~year time-window ~~is of less than 5%.~~.

We suggest here a comprehensive method to evaluate rockfall hazard where only past rockfall evidence exists in the field. We show the importance of integrating spatial and temporal field-observations to assess the extent of rockfall hazard, the potential block size-distribution, and the rockfall recurrence interval.

## 1 Introduction

Rockfalls are a type of fast mass movement process common in mountainous areas worldwide (Dorren, 2003; Flageollet and Weber, 1996; Mackey and Quigley, 2014; Pellicani et al., 2016; Strunden et al., 2015; Whalley, 1984). In this process, a fragment of rock is detached from ~~the bedrock~~a rocky mass along a pre-existing ~~discontinuities~~discontinuity (e.g., bedding, fractures) slides, topples or falls along a vertical or nearly vertical cliff. Individual fragments travel downslope by bouncing and flying or by rolling on talus or debris slopes (Crosta and Agliardi, 2004; Cruden and Varnes, 1996; Varnes, 1978; Whalley, 1984, Wei et al., 2014). ~~They travel at speeds of a few to tens of meters per second, and range in volume up to thousands of cubic meters.~~The rock fragments travel at speeds of a few to tens meters per second, and range in volume up to thousands of cubic meters. Different mechanisms are known to trigger rockfalls: earthquakes (Kobayashi et al., 1990; Vidrih et al., 2001), rainfall and freeze-and-thaw cycles (Wieczorek and Jäger, 1996; D'amato et al., 2016). Due to their high mobility, and despite their sometimes small size, rockfalls are particularly destructive mass movements, and in several areas they represent ~~the~~a primary cause of landslide fatalities ~~(Evans, 1997; Evans and Hungr, 1993~~(Evans and Hungr, 1993; Evans, 1997; Guzzetti, 2000; Keefer, 2002; Guzzetti et al., 2003; Guzzetti et al., 2005~~);~~ Badoux et al., 2016)~~.~~. In mountainous areas human life and property are subject to rockfall hazard (Crosta and Agliardi, 2004) and efforts are made to mitigate the hazard. Mitigation measures for rockfall damage are primary based on hazard assessment, which integrates all available data to map and scale the hazard (e.g. Guzzetti et al., 2003). The spatial extent of the hazard in many cases can be resolved using field observations of documented historical rockfalls (Wieczorek and Jäger, 1996) and computer modeled trajectories (Dorren, 2003 and references therein). The temporal aspect of hazard and the triggering mechanism usually rely on historical reports, but rarely on direct dating of past rockfall events (e.g. De Biagi et al., 2017; Kanari, 2008; Rinat et al., 2014). However, hazard estimation where no historical documentation of past rockfalls exists (hence no documentation of neither the spatial and temporal extents), nor any knowledge of the triggering mechanism, such as the case presented here, is rare or missing in literature.

The current study evaluates the rockfall hazard for the town of Qiryat-Shemona (northern Israel), by (a) studying the extent and nature of past rockfall events using field observation; (b) Constraining the date of the rockfall events and their reoccurrence interval using optically stimulated luminescence (OSL) dating (Wintle, 2008).~~The town of Qiryat-Shemona (northern Israel;~~ The possible temporal relation to known historical earthquakes, which might serve as a trigger, is also studied; (c) computer-modeling the most probable down-slope rockfall trajectories which outline the hazard-prone area. Particular attention is given to the calibration of the computer modeling using mapping of past rockfall events and extracting geometrical and mechanical parameters needed for the simulations from the field observations. This study presents a methodology for rockfall hazard estimation where field evidence for past rockfalls are observed in the town vicinity, but the triggering mechanism, the timing of past rockfall events and recurrence intervals are entirely unknown.

## 2 Study Area

The town of Qiryat-Shemona (population 25,000) is located in the northern Hula Valley (Fig. 1), one of a series of an extensional basins developed along the active left lateral fault system of the *Dead Sea Transform* (DST) (Freund, 1965; Garfunkel, 1981; Quennell, 1958). The town is built at the foot of the fault-controlled Ramim escarpment, which rises 800 meters above the west part of the town. New quarters of the town are being planned and built below the escarpment and up the slopes above the town. These slopes are dotted with cliff-derived boulders with measured volumes of more than 100 $m^3$, which have apparently traveled down the slope by rockfall mechanism (Fig. 2). Pre-town aerial photos (dated ~1945) reveal additional rock blocks with similarly estimated volume-range within the now built town premises. Thus, the field observations and aerial photos interpretation suggest that the western neighborhoods of Qiryat-Shemona, located at the escarpment base, are subjected to rockfall hazard.

~~The current study aims to evaluate the rockfall hazard for the town of Qiryat-Shemona by (a) studying the past rockfall events, (b) identifying the rockfall triggering conditions and their reoccurrence interval, (c) computer-modeling the most probable down-slope rockfall trajectories which outline the hazard-prone area, and (d) by calculating the expected kinetic energy of the blocks at the town borders. Particular attention is given to the calibration of the computer-modeling using mapping of past rockfall events and extracting geometrical and mechanical parameters needed for the simulations from the field observations. The age of the studied past rockfall events and their possible relation to known historical earthquakes are constrained by optically stimulated luminescence (OSL) dating (Wintle, 2008).~~

## ~~2 Study Area~~

The rock sequence outcrops in the lower part of the slopes, west of the town (hereafter 'the study area'; Fig. 1b) consists of Lower Cretaceous rocks (Glikson, 1966; Kafri, 1991;): The sandstone of Hatira Formation outcrops at the base of the slope, overlain by limestone and marl of Nabi Said Formation. Further up-slope, about 350 m above the town, outcrops the biomicritic limestone of Ein-El-Assad Formation, creating a 40 m high sub-vertical cliff (Fig. 2). This cliff is the source for rockfalls in the study area (see below). The Ein El Assad Formation is overlaid by a ~700 m Lower to Upper Cretaceous carbonate rocks (Sneh and Weinberger, 2003a, b). Colluvium and rock-mass movement deposits were mapped on the slopes near Qiryat-Shemona (Shtober-Zisu, 2006, Sneh and Weinberger, 2003a)~~.~~, identifying the blocks on the slope as originating from the Ein-El-Assad formation. The slopes are generally covered with up to a few meters of soil. The studied area is located along a primary fault zone of the DST (Weinberger et al., 2009). ~~Here the western-border fault of the Hula basin branches into several faults towards the north.~~

Large historic and prehistoric earthquakes (M >6.5) along the DST are well documented: Ben-Menahem (1991), Amiran et al. (1994), Guidoboni et al. (1994), Guidoboni and Comastri (2005), Marco et al., 2003, Marco et al., 2005, Marco et al., 1996, ~~and~~ Katz et al., (2010~~).~~) and Wechsler et al., (2014). Recurrence intervals for $M_W$ = 6.5 and $M_W$= 7.0 earthquakes ~~is~~was calculated to 800 and 3000 years in accordance (Begin, 2005)~~.~~, while another study suggests that the average recurrence interval for a large earthquake (M ≥6.5) in this segment of the DST is ~1500 yr (Hamiel et al., 2009). Some of the significant historical earthquakes induced slope failures (Katz and Crouvi, 2007; Wechsler et al., 2009; Yagoda-Biran et al., 2010).

## 3 Methods

### 3.1 Rock block inventory

~~A~~In a given site, the size distribution of boulders resulting from past local rockfalls (recent or historical) is the best database for assessing predicted rockfall block size. Thus mapping the blocks is crucial for hazard analysis, as suggested by previous studies that required estimations or measurements of the number of blocks and their volumes (Brunetti et al., 2009, Dussauge-Peisser et al., 2002; Dussauge et al., 2003; Guzzetti et al., 2003; Malamud et al., 2004; Katz and Aharonov, 2006; Katz et al., 2011). In this study, a catalog of the past-rockfall derived boulders was constructed from two data sources: 76 blocks were mapped and measured in the field ~~and~~ with volumes varying between 1 $m^3$ and 125 $m^3$. Additional 200 blocks were mapped using pre-town aerial photos (dating to 1946 and 1951). 58 out of the 200 blocks mapped using the aerial photos were identified and measured in the field as well (green rectangles in Fig. 3). These ~~58~~ blocks~~, which were identified both on the aerial photos and measured in the field~~, were used to fit a correlation curve between field measured and aerial photo estimated block volumes. The correlation was used for volume estimation of the blocks that were removed from the area during the ~~establishment~~construction of the town, but were mapped on the aerial photos predating the establishment (142 blocks out of 200).

In summary, the catalog ~~host~~hosts a total of 218 boulders, which were mapped and their volumes were measured or estimated from aerial photos. This rock block inventory is the basis for the prediction of probabilities for different block sizes for the calculation of rockfall hazard and its mitigation.

### 3.2 Rockfall simulations

The down-slope trajectory of a rock-block (or the energy dissipated as it travels) is affected by ~~slope~~the geometry and ~~surface material~~physical properties of the slope and ~~by the rock-block geometry and material properties~~the detached blocks (Agliardi and Crosta, 2003; Guzzetti et al., 2002; Guzzetti et al., 2004; Guzzetti et al., 2003; Jones et al., 2000; Pfeiffer and Bowen, 1989; Ritchie, 1963). Parameters that quantify these measures are used as input for computer-simulation of rockfall trajectories.

Several computer programs have been developed and tested to simulate rockfall trajectories~~: (Guzzetti et al. (2002); Dorren, 2003 and references therein; Giani et al., (2004)~~Guzzetti et al., 2002; Dorren, 2003 and references therein; Giani et al., 2004)**.** The current study uses the 2D Colorado Rockfall Simulation Program, CRSP, v4 (Jones et al., 2000) to analyze two significant aspects of rockfall hazard in the studied area: First, the expected travel distance of rock-blocks along the studied slopes, which signifies the urban area prone to rockfall hazard. Second, the statistical distributions of block travel velocities and kinetic energy, which serves as an input for engineering hazard reduction measures. For the current analysis the model input parameters are the topographic profile of the slope (extracted from 5 m elevation contours GIS database and verified in the field), surface roughness (S), slope rebound and friction characteristics, ($R_n$: normal coefficient of restitution; $R_t$: tangential coefficient of frictional resistance) and block morphology. S was measured in the field according to Jones et al., (2000) and Pfeiffer and Bowen, (1989), where $R_n$ and $R_t$ were estimated via a calibration process (see below).

The CRSP algorithm simulates rockfall as a series of rock-block bounces, and calculates the changes in the block velocity after each impact with the slope surface, taking into consideration the rock and slope geometric and mechanical properties. Model output is a statistical distribution of velocity, kinetic energy and bounce height along the downslope trajectory, including stopping distances of the blocks (Jones et al., 2000). The slope surface in CRSP is divided into slope cells, which boundaries are defined where the slope angle changes, or where the slope roughness changes (Jones et al., 2000).

For the current study, we simulated the rockfalls characteristics along topographic profiles extending from the Ein-El-Assad Formation, identified as the source for the rockfalls, downslope towards the town. 25 topographic profiles covering the study area were extracted for the rockfall hazard analysis (Fig. 4), with high spatial density (30–100 m intervals) where the source for rock-blocks is exposed above the town and lower spatial density (150–500 m intervals) further southwards. A single simulation run (along each profile) modeled 100 rock-blocks, thus allowing the statistical analysis (Jones et al., 2000). CRSP results for each profile were later integrated spatially to compile rockfall hazard maps and other hazard properties as detailed below. The simulated block volumes were binned into size scales of 1, 10, 50, 100, 125 $m^3$, with corresponding block diameters of 1.3, 2.7, 4.6, 5.8 and 6.2 m, respectively (assuming spherical block geometry).

### 3.3. CRSP calibration

The first step in hazard analysis using a computerized model is calibration of the model input parameter. Following Katz et al. (2011), calibration was performed by comparing calculated traveling distance of rock blocks of a given size to field observed ones, while adjusting the assigned model-parameters until best-fit was obtained, i.e., back-analysis.

In the current work, CRSP calibration using back-analysis was performed along four slopes ~~with~~(pink lines in Fig. 3) located at the N and S parts of the prominent Ein-El-Assad source outcrop, where a relatively high number of field mapped (50 blocks out of 76) and aerial photo mapped rock-blocks (~~pink lines in Fig. 3).~~65 blocks out of 200) were observed. As an index for calibration quality, we used the difference between the *field-observed* down-slope maximal travel distance along a selected slope and the *simulated* maximal travel distance along this slope (hereafter $\Delta MD$ in meters), for a given block-size bin. We

considered the model parameters as calibrated when $\Delta MD$ = ±60 m (about 10% of average profile length). 80 simulation runs, modeling the largest blocks with diameters of D of 5.8 m and 6.2 m along the four profiles were used for calibration (Determined S value is 0.5 for D=5.8 and 6.2 m). These simulations resulted in the following coefficient value ranges: $R_n$=0.2~~–~~ ~~–~~ 0.25; $R_t$=0.7~~–~~ ~~–~~ 0.8, which are in agreement with suggested values for bedrock or firm soil slopes according to Jones et al. (2000). These values were further revised and refined following the initial velocity sensitivity analysis (detailed in the following).

The predicted seismic peak ground acceleration (PGA) for the studied area is 0.26 g (Shapira, 2002). Assuming a PGA ($a$) of 0.3 g with frequency ($f$) of 1 Hz (Scholz, 2002), the calculated initial horizontal velocity (~~$V_x$~~$U_x$) of the rock block is 3 m/s (~~$V_x$~~$U_x$ = $a/f$). Sensitivity analysis was performed for two end members of ~~$V_x$ of~~ $U_x$ =0 m/s (simulating a-seismic triggering of a rockfall) and $U_x$ =3 m/s (simulating seismic triggering). Where, $R_n$ = 0.12 yielded $\Delta MD$ = -90 m and -80 m for ~~$V_x$~~$U_x$ = 0 m/s and ~~$V_x$~~$U_x$ = 3 m/s, respectively; and $R_n$ = 0.25 yielded $\Delta MD$ = +160 m and +150 m for ~~$V_x$~~$U_x$ = 0 m/s and ~~$V_x$~~$U_x$ = 3 m/s, respectively**.** Thus, we infer that initial velocity has no significant effect on travel distance. An exponential regression curve was fitted for ~~$\Delta MD$ vs.~~the above $R_n$ values (~~at $V_x$ =~~ 0.12, 0.2, 0.25) vs their corresponding $\Delta MD$ values (-90, -30, +160 m~~/s~~), which ~~yields~~yielded $\Delta MD$ = 0 m (minimum difference between observed and simulated maximum travel distance) at $R_n$ = 0.22. Thus, calibration ~~is satisfied~~was determined optimal for $R_n$ = 0.22. We estimate that 0.01 change in Rn will yield 15-30m change in maximum travel distance. Calibration profiles are 450 m-750 m, yielding 2%-3% variability for 0.01 change in $R_n$. CRSP output is less sensitive to changes in the tangential coefficient $R_t$ in comparison to changes in the normal coefficient $R_n$. Hence $R_t$ value was determined to 0.~~7 using~~70 following our initial calibration~~. This~~ value, which is also recommended by Jones et al (2000) for firm soil slopes.

~~Further~~To validate these coefficients, further simulation runs along the four calibration profiles were performed for all block sizes (D~~= =~~ 1.~~3 3~~m~~-~~6.2 m), using the above detailed best-fit ~~coefficient~~ values~~:~~ $R_n$ =0.22; $R_t$ =0.70 and the field-measured surface roughness S values S=0.1, 0.3, 0.4 m for block diameters D=1.3 m, 2.7 m, 4.6 m respectively, and S=0.5 m for D=5.8 and 6.2 m (all S values were measured in the field per block diameter~~); $R_n$ =0.22; $R_t$ =0.70.~~ according to CRSP software manual). All slope cells were given the same values to maintain model simplicity. The travel distances of simulation results were compared with the observed travel distances (from field mapping and aerial photo mapping). The fit between observation and simulation is plotted in Fig. 5. These results can be divided into two behavior patterns: *(a) mid-size and large blocks* (D ≥3 m; green, orange and red circles): the observed and simulated results are close to the 1:1 ratio; for large blocks (D ≥4 m), simulated travel distance is a little longer, which yields a more conservative result. *(b) small blocks* (D< 3 m): some blocks are close to the 1:1 ratio, while others demonstrate significantly longer *observed* travel distances. This longer observed than simulated travel distance of smaller blocks ~~(D< 3m)~~ may be explained in a few ways: First, smaller blocks may be more subject to creep, being more affected by water runoff and slope material movement due to their lower weight. Therefore they may travel further down after the rockfall event took place. Another possible interpretation is that the construction of town has created a different topographical setting than the slope at the time of rockfall events in the past. To circumvent this discrepancy for the hazard analysis, we use only the larger blocks.

Sensitivity analysis for block shape resulted in an insignificant difference between simulations done with sphere, disc or cylinder rock-block shapes. Accordingly, we used sphere shape rock-blocks in the prediction simulations because they yield maximum volume for a given radius and thus tend toward a worst-case scenario analysis (Giani et al., 2004; Jones et al., 2000).

### 3.4 OSL age determinations

For OSL age determinations of rockfall events, colluvium or soil material from immediately underneath the rock blocks was sampled. This approach constrains the time since last exposure to sunlight before burial under the blocks (following Becker and Davenport, 2003). For sampling we excavated a ditch alongside the rock block to reach the contact with the underlying soil using a backhoe, then manually excavated horizontally under the block and sampled the soil below its center. The Sampling

of soil was performed under a cover to prevent sunlight exposure of the soil samples. A complementary sediment sample was taken from each OSL sample location for dose rate measurements. Locations of sampled blocks are marked in Fig. 3. Rockfall OSL age determination was based on the assumption that the sampled blocks did not creep or remove from their initial falling location. Thus, only very large blocks between 8 and 80 $m^3$, weighing tens to hundreds of tons, were sampled. OSL equivalent dose De was obtained using the single aliquot regeneration (SAR) dose protocol, ~~using a range of~~ with preheats ~~(~~of 10 s @ 220~~—~~260°C~~)~~ and a cutheat 20° below preheat (Murray and Wintle 2006). ~~The gamma and cosmic dose rates were~~"No. of discs" is the number from those measured that was used for calculating the De. Over-dispersion (OD) is an indication of the scatter within the sample beyond that which would be expected from experimental uncertainties. Ages calculated using the Central Age Model after rejection of outliers. Gamma dose rates measured in the field using ~~a calibrated~~the gamma counter are lower than gamma ~~scintillator. Alpha and beta~~ dose rates ~~were~~ calculated from the ~~concentration~~concentrations of K, U~~,~~ and Th~~, and K in the complementary sediment sample.~~ (with the cosmic dose calculated from burial depth).

## 4 Results

### 4.1 Size distribution of rockfalls

Rock-blocks, a result of rockfall events, are commonly observed along the slope west of Qiryat Shemona, at the foot of the Ein-El-Assad Formation. Their volume varies, from the smallest pebbles to boulders tens of cubic meters in volume. In places the blocks form grain-supported piles, revealing impact deformations on their common faces such as chipped corners and imbricated blocks separated along previous fracturing surfaces. To determine rockfall hazard and risk, information on the frequency-volume statistics of individual rockfalls is necessary (Guzzetti et al., 2004; Guzzetti et al., 2003).

We used the field mapped blocks to determine their volume distribution. In total, we consider this field catalog complete for block size >1 $m^3$ and consists of 76 blocks ranging in volume up to 125 $m^3$ (mode~~=~~ = 56~~.25~~ $m^3$). Following Malamud et al. (2004), the volume distribution of the mapped blocks ~~can be~~is determined using the probability density, *p,* of a given block volume Eq. (1):

$$p = \frac{dN}{NdV} \sim V^{\alpha} \qquad (1)$$

where N is the total number of blocks, dN is the number of blocks with volume between V and V+dV, and α is the scaling exponent. Our results show that the volume of the individual rock blocks from the studied area exhibits a distinct negative power law behavior, with a scaling exponent of the right tail of α = -1.17 ($R^2$ = 0.72; Fig. 6). This conforms to what was found by others who examined natural rockfalls with observed α ranging: -1.07 - -1.4, e.g., Guzzetti et al. (2003) Malamud et al. (2004) Brunetti et al. (2009). The scaling exponent is also similar to the value α = -1.13 obtained experimentally by Katz and Aharonov (2006), while Katz et al. (2011) found a larger scaling exponent, α = -1.8.

Since our data yield a moderate inner consistency $R^2$=0.72 we round the power to -1.2 (instead of -1.17). In accordance, the probability density function (PDF) for rockfall volume (*p)* may be presented as a power law of the form (Dussauge-Peisser et al., 2002; Dussauge et al., 2003; Guzzetti et al., 2003; Malamud et al., 2004) Eq. ~~(2):~~(2), where *V* is the given block volume in $m^3$:

$$p = 0.4V^{-1.17} \qquad (2$$

~~where *V* is the given block volume. The power law is -1.17 and $R^2$ = 0.72 (for the 76 field mapped blocks plotted in Fig. 3).~~

To simplify the hazard evaluation~~,~~ and relate to the more prominent hazard which larger block sizes impose (thus removing the 1 $m^3$ smaller blocks from the simulation runs) the block volumes were binned into size scales of 10, 50, 100, 125 $m^3$, with corresponding block diameters of 2.7, 4.6, 5.8 and 6.2 m~~,~~ respectively (assuming spherical block geometry). ~~Cumulative~~Field mapped cumulative frequencies were used to derive cumulative probabilities for each block size (Table 1). The probability

values per block diameter (Table 1) were fitted a regression curve in Excel ($R^2 = 0.97$), yielding the probability ($p_D$) for a block of given diameter ($D$) or smaller following Eq. (3):

$$pD = 0.412Ln(D) + 0.262 \quad (3)$$

The cumulative probability calculated from Eq. (3) per block diameter differs from the cumulative probability calculated in Eq. (2) per its matching block volume because of the differences in data-sets and usage of the two equations: Eq. (2) power-law details our full field-observed data of block sizes and is used to characterize the dataset and compare it to other block catalogs in other studies. While Eq. (3) yields a simulation-specific empirical prediction for probability of occurrence for the larger block diameters (D>=2.7 m; V>=10 m$^3$), which were actually used later in the CRSP simulations for hazard analysis.

### 4.2 Simulations of block trajectories

For the hazard analysis, we ran computer simulations along 25 profiles including the four profiles used for the calibration (Fig. 3), using the calibrated parameters and the measured topographic-profiles as the model input. A total of 100 computer runs~~, each run simulating the fall of 100 individual blocks,~~ were performed (four runs on each of the 25 profiles~~:~~, using block dimeters of 2.7, 4.6, 5.8, and 6.2 m separately~~,~~), each run simulating the fall of 100 individual blocks (totaling 10,000 simulated single block trajectories). These results were used to analyze the hazard in the study area.

#### 4.2.1 Stop angle and stop swath

The *'x% stop angle*' is defined as the slope angle of the profile cell at which cumulated x% of simulated blocks stop and, in accordance, the *'stop swath'* is defined as the distance (m) ~~along the profile cell with the corresponding to stop angle~~ that the simulated blocks covered until all of them (100%) stopped. ~~For a~~Example: if the total 100% ~~stop angle, all traveling~~of the simulated blocks ~~will stop~~stopped within a profile cell that has 5° slope and the last one of them stopped after covering 65 meters along that cell – the *100% stop angle* is 5° and the *stop swath* ~~distance~~is 65 m. The 50% and 100% stop angle and stop swath data were extracted from the CRSP simulation analysis (Fig. 7). 100% stop angles for all profiles (red circles in Fig. 7) ~~have~~ vary between 3°-12° with a mean of 7.7° ~~with~~and *SD* = 2.3° (~~range of 3°-12~~1σ=6.4°-10.0°); 50% stop angles (blue triangles) ~~have~~ vary between 3.2°-25.8° with a mean of 10° ~~with~~and *SD* = 5.3~~°~~.° (1σ=4.7°-15.3°). All other cell slope angles in all profiles (gray circles) vary widely between 7°-88~~°, among~~° with a mean of 29.4° with *SD* = 17° (1σ=12.4°-46.4°). Among them very few are less than 10°. Stop swath distances range between 8~~ m to~~ 105 m, ~~having~~with a mean of 38 m ~~with~~and *SD* = 24 m~~.~~ (1σ=14-62 m). Only in two profiles (out of 25) did the stop swath distance exceed 65 m. In both these cases, 100% stop angle is steeper than in most other profiles (10°-11°). Further details and illustration for slope cells and stop angles are given in Fig 7. No significant correlation was found between 100% stop angle and stop swath distance.

#### 4.2.2 Rockfall hazard

Rockfall hazard map for Qiryat-Shemona is presented in Fig. 8. The hazard map was compiled from the simulated maximal travel distance (where 100% of blocks stop) of the largest blocks (D >4.6 m, V >50 m$^3$) with the probability of occurrence, *pD* = 11% (Eq. 3). The calculated block trajectories cross the town border and mark the town premises that are subject to rockfall hazard along 8 out of 25 simulated profiles (#8~~ # –~~ #14 and #16, marked by † in Fig. 9). The area subjected to rockfall hazard is about 1.55 km$^2$, currently including several houses (according to the last updated google Earth image from Nov 2014). For D=4.6 m, block impact velocity varies between 9.5–13.7 m/s and kinetic energy between 7,400–16,300 kJ (Table 2). CRSP simulated maximal travel distance and CRSP velocity and kinetic energy analysis points at town border impact locations are plotted in Fig. 9. ~~For details of the kinetic analysis see locations marked by profile indexes and~~Yellow line represents the CRSP 100% stop line calculated for large blocks (D is 5.8 m and 6.2 m). Yellow-black triangles mark simulated stop points; Orange-black triangles mark simulated town border impact points (those labeled with a sword '†' mark locations of rockfall

impact at town border) where kinetic energy was calculated. For details of the kinetic analysis at these locations refer to Table 2.

### 4.3 OSL age determination of rockfalls

OSL ages were determined for ~~eight~~nine rock blocks~~.~~ with volume range of 8 $m^3$ - 80 $m^3$. The ~~locations~~location of these blocks is marked in red circles in Fig. 3. These ages range from 0.~~7~~9 to ~~8.1~~9.7 ka, with uncertainties of ~~9-40~~6% - 14% (Table 3).

## 5 Discussion

### 5.1 Triggering conditions for rockfalls in the studied area

We interpret the field observed grain supported structure of aggregations of blocks of various sizes, with impact deformations (e.g., chipping) on their common faces as evidence for catastrophic events, involving numerous blocks. Long-term erosion which results in single sporadic block failures would have resulted in matrix-supported blocks and not in the evidence observed here. We conclude that the rockfalls were mainly triggered by discrete catastrophic events such as earthquakes or extreme precipitation events. The question of a triggering mechanism in the case of a catastrophic rockfall event is an important one when attempting to evaluate the temporal aspect of rockfall hazard. The recurrence time of an extreme winter storm or a large earthquake may give some constraints on the expected recurrence time of rain-induced or an earthquake-induced rockfall, respectively. Furthermore, it might suggest a periodical probability for the next rockfall to occur when hazard is calculated. The correlation of rockfall events to historical extreme ~~rainstorms~~rainstorm events is limited due to the lack of long enough historical rainstorm record. ~~Noticeably, even following~~However, in the 74 years of documented climatic history for the studied area (measurements at the 5 km away Kfar-Blum station since 1944; IMS, 2007) no significant rock-mass movements and rockfalls were reported in the study area. Thus period includes the extremely rainy winters of 1968/69 and 1991/92, in which annual precipitation in northern Israel was double than the mean annual precipitation (IMS, 2007)~~, no significant rock-mass movements and rockfalls are reported in the study area. Thus, rainstorms are ruled out as a favorable triggering mechanism.~~. Furthermore, the winter of 2018-2019 (during which the current study is being prepared for publication) breaks a five-year drought that was the worst Israel has experienced in decades (Time of Israel, 2019), with massive floods, snowfall, overnight freeze and rainstorms in Northern Israel, including in the study area. The authors of the current study received 1st-hand personal correspondence (photos, videos and descriptions) from hikers on the studied slope, which observed some dismantling of rock blocks in their location during one of the large rainstorms in Jan-2019. Yet no rockfall events were documented in the study area during this extreme winter season. Contrastingly, Wieczorek and Jäger (1996) reported that out of 395 documented rockfall events in the Yosemite Valley which occurred between 1851 and 1992, the most dominant recognized trigger for slope movement was precipitation (27% of reported cases), and point out the influence of climatic triggering of rockfall. Based on this significant difference of observations for rockfall triggering mechanisms, we suggest that rainstorms may not provide a major triggering mechanism for rockfalls in our study area. A possible correlation between the dated rockfall events and historical earthquakes is analyzed below.

### 5.2 Non-random temporal distribution of rockfalls and correlation to earthquakes

The following discussion relates to blocks of sizes equal or larger than 8 $m^3$ (D>2.5 m) as the OSL dated blocks were of sizes 8-80 $m^3$). These volumes fit the CRSP simulation analyses of all blocks in the study, as the smallest simulated block for the hazard estimation was 10 $m^3$ (D=2.7 m).

The wide range of OSL ages, between ~~700~~0.9 ka and ~~8100 years~~9.7 ka before present (Fig. 10 and Table 3), rules out the possibility of a single rockfall event. Given the rich historical earthquake record in the vicinity of the studied area, the positive

correlation between rockfall events and historical earthquakes may shed light on the triggering mechanism of the rockfalls. A similar approach was used by Matmon et al. (2005), Rinat et al. (2014) and Siman-Tov (2009)~~, who~~. The latter dated rockfall events ~~~~30 km SW ~~from~~of the studied area, where he found a positive correlation between rockfall events and historical earthquakes, dated 749 AD and 1202 AD. To ~~perform~~analyze this possible correlation, we overlaid the ~~8~~9 OSL ages with a set of 9 large historic earthquakes ~~that occurred in the vicinity of the study area~~ (Table 4, Fig. 10~~). This set contains earthquakes that~~), which comply to these cumulative terms: (a) occurred within the time spans of the OSL ages; ~~-~~(b) their maximum estimated intensity is at least 'IX' ~~on an~~in EMS ~~macroseismic local intensity scale~~(European Macroseismic Scale) and/or their estimated moment-magnitude is 6 or larger; (c) the distance between ~~the~~our study area and affected localities ~~reported~~ does not exceed 100 km (following Keefer, 1984).

The ~~8~~9 OSL ages (Table 3; Fig. 10) span over the past ~~8000~~9700 years with a mean of one ~~age~~occurrence per 1,000 years. The validation of OSL age clustering was obtained performing a binomial distribution test, which gives the discrete probability distribution *P(k,p,n)* of obtaining exactly *k* successes out of *n* trials. The result of each trial is true (success) or false (failure), given the probability for success *(p)* or failure *(1-p)* in a single trial. The binomial distribution is therefore given by Eq. (4):

$$P(k,p,n) = \binom{n}{k} p^k (1-p)^{n-k}, \quad where \binom{n}{k} = \frac{n!}{k!(n-k!)} \qquad (4)$$

A 'success' was defined when the date of a given earthquake (out of the nine candidates in Table 4) with a ±50 years time window, coincides in time with one of the OSL ages with the same error range (±50 years). Since the selected limited time window is ±50 years (±0.05 ka), the test was performed only for OSL ages that correspond to relatively accurate historically recorded earthquakes (last 2,800 years): 759 and 199 BC, 363, 502, 551, 659, 749, 1033 and 1202 AD. The OSL ages within this range are of QS-3 (1.~~5~~6±0.~~13~~1 ka), QS-4 (1.0~~.89~~±0.~~16~~1 ka), QS-6 (2.~~2~~1±0.~~50 ka), QS-9 (3.0±1.~~2 ka) and QS-11 (~~2.2±0~~1.7±0.2 ka). The selected nine historical earthquakes, each with a ±50 year time window, span over 900 years out of the given 2,800 years period (for each event, a ±50 year time window spans 100 years). Therefore, the probability *p* for a single random earthquake to occur within this period is *p* = 900/2800=0.32. The number of trials *n* is the number of earthquakes *n* = 9. In five cases (the earthquakes of 199 BC, 363 AD, 502 AD, ~~551 AD,~~ 1033~~ AD, 1202~~ AD), a success (match between an earthquake and an OSL age) is obtained~~,~~ (363 AD matches two OSL ages QS-3 and QS-11), therefore the number of successes is *k* = 5. This fit between OSL ages and earthquakes is detailed in Fig. 11. Accordingly, the binomial distribution is *P(k, p, n)*= *P*(5, 0.32, 9) = 0.09, i.e., there is a 9% probability to randomly obtain such a distribution of events in time ~~randomly~~. Hence, we suggest that the OSL age distribution is significantly clustered around dates of the discussed historical earthquakes, with 91% confidence level, thus suggesting a likelihood of seismic triggering for the rockfalls in the studied area. Assuming that ~~magnitude six~~M>6 earthquake ~~or larger is~~ needed for rockfall triggering (following Keefer, 1984) and based on the recurrence time of 550 years given for these earthquakes (Hamiel et al., 2009), we predicted a ~550 years recurrence time for rockfalls in the studied area.

Not all historic earthquakes are represented in our OSL data set, such as the 1759 AD (Ambraseys and Barazangi, 1989; Marco et al., 2005) and 1837 AD (Ambraseys, 1997; Nemer and Meghraoui, 2006) earthquakes, which both induced extensive damage to cities not far from the ~~studied~~study area (Katz and Crouvi, 2007). This lack of evidence could be explained by OSL under-sampling, or because earthquakes only trigger rockfalls that were on their verge of ~~stability~~instability (Siman-Tov et al., 2017).

Based on the above analysis we correlate the past rockfalls to historic earthquakes as follows:

~~a. QS-4 (0.89±0.16 ka) fits the historical earthquakes of 1202 AD or 1033 AD. Since the 1202 AD earthquake accounts for severe damage in other places in northern Israel (Marco et al., 1997; Wechsler et al., 2006), we find it a better candidate for triggering a rockfall event than the 1033 AD event.~~

~~b. QS-3 (1.5±0.13 ka) fits the historical earthquakes of 502 AD and 551 AD. The 551 AD earthquake is reported at more localities along the DST than the 502 AD (reported on shoreline localities only). Hence we find it a better rockfall triggering candidate.~~

c. QS-6, QS-9 and QS-11 cluster around 2.2 ka, which fits the 199 BC earthquake.

a. QS-9 (3.0±1QS-4 (1.0±0.1 ka ) fits the historical earthquake of 1033 AD.

b. QS-3 (1.6±0.1 ka ) and QS-11 (1.7±0.2 ka) fit the historical earthquakes of 363 AD and 502 AD, and only lack ~40 years in error margin to fit the one of 551 AD. Since the 502 AD was reported on shoreline localities only in the DST area, we find the 363 AD a better rockfall triggering candidate. We suggest that the two ages are clustered around one of these earthquakes, hence suggesting they represent one rockfall event in the 363 AD earthquake. however, we cannot completely rule-out the possibility that these were two separate rockfall events, both triggered by large earthquakes in 363 AD and 502/551 AD.

c. QS-6 (2.1±0.2 ka) fits the 199 BC earthquake and .

d. QS-13 (3.2±0.4 ka) lacks ~30 years in error margin to fit the 759 BC earthquakes QS-9 also fits the 2050-2100 BC earthquake.

e. QS-5 (4.0±0.707 ka), QS-9 (4.3±0.6 ka) and QS-12 (4.1±0095±0.4 ka) fit the 2050/2100 BC earthquake (or two separate events) suggested by Migowski et al. (2004). This also fits the findings of Katz et al. (2011) and Yagoda-Biran et al. (2010), who found evidence for earthquake and earthquake-induced slope failure east of the Sea of Galilee (ca. 50 km south from study area, along the DST) with OSL ages of 5.0±0.3 and 5.2±0.4 ka, respectively, suggesting the area had experienced one or more strong earthquakes. We therefore suggest that these OSL ages cluster around a single rockfall event triggered by a large earthquake within the period of 3.7-4.9 ka.

f. QS-1 is (7.0±1.1 ka) may correlate with the Mw=7 earthquake derived from slope movement evidence dated by Yagoda-Biran et al. (2010) to 6.0±0.4 ka east of the Sea of Galilee.

f. QS-1 (8.7±1.0 ka) may correlate with an earthquake event suggested by Daeron et al. (2007) on the Yammunneh Fault in Lebanon dated to 8.4–9.0 ka (identified in a paleoseismic trench 50 km north of the study area).

### 5.3 Rockfall hazard for the town of Qiryat Shemona

#### 5.3.1 Area subject to rockfall hazard

The nature of the analyzed past rockfall events in the studied area can be used to constrain the possible characteristics of the expected future rockfall events and promotedirect hazard mitigation. The predicted probabilities $P_D$ for specific rock fall with a given block diameter or smaller, derived from the regression curve *(Eq. 3)*, are presented in Table 1. $P_D(2.7)$, the cumulative probability for a block of D = 2.7 m (V = 10 m$^3$) or smaller is 0.67. Consequently, the probability for traveling blocks of 2.7< D< 6.2 m (10< V< 125 m$^3$), is $1\text{-}P_D(2.7)$ = 0.33 or 33%. The occurrence of larger, more destructive blocks amongst these (D = 4.6 m - 6.2 m or respectively, V = 50 - 125 m$^3$) is $P_D$ = 11%. Despite their lower probability, these blocks would reach the farthest distances; and hence pose the largest hazard to town.

The area subjected to rockfall hazard for travel distances of the large blocks (D = 4.6-6.2 m, V >50-125 m$^3$, 11% probability) appears in Fig. 8. About 50,000 m$^2$ (0.05 km$^2$) of the westernmost, currently inhabited and built, urban area (out of 1.55 km$^2$ total area mapped as subject to rockfall hazard, which also includes the above town slope outside the urbanized area) is mapped under direct rockfall impact hazard.hazard (considering the large blocks: D = 4.6 m - 6.2 m), as well as the slopes above this part of the town (Fig. 8). This hazard mapping may be used to plan mitigation actions and also as a basis for future urban planning.

We note that the main road connectionconnecting the town southwards, which can serve as evacuation route, is not under highmarginally beyond the rockfall hazard. mapped zone (Fig. 8). We also note that some smaller blocks (D≤ 3 m) were mapped from the historical aerial photos predating town establishment further down slope below the simulated 100% blocks stop (Fig. 3; blue circles in Fig. 65). As suggested above these might be blocks that traveled farther downslope by creeping after the rockfall event. Another possible explanation is that these now inhabited parts of the slope were altered and even levelled by the construction works. Hence the simulated profile extracted from current topography is different from the slope

topography on which these smaller blocks traveled before the construction of town. No detailed topography maps pre-dating town establishment is available to verify this.

The stop angle results (Fig. 7) indicate that most blocks (>50%) keep traveling down-slope until the slope angle decreases to 10°-15°. All blocks stop where the slope angle decreases to values between 5.5°-10.0°. Combined with the stop swath distance results (Sect. 4.2.1 above), considering the means and SD's, CRSP results indicate that falling blocks would stop after covering a distance of 14~~-~~ m~~-~~ 62 m from the source on a slope angle of 5°-10° at the point of stopping. This conclusion may help when considering rockfall mitigation design.

### 5.~~3.2~~4 Rockfall hazard probability

~~We~~We discuss the hazard probability by addressing three terms: time dependency, size dependency and susceptibility.

**Time dependency:** we derive the recurrence time for rockfalls in the study area by correlating OSL dating of rockfall events to past earthquakes, as detailed above. Thus, we can calculate the probability of a rockfall occurrence $P_{EQ}$ in the next 50 years, assuming earthquake magnitude ~~M =~~Mw = 6 as the threshold for rockfall: $P_{EQ}$ = 50/550 = ~0.09 or 9%. We do not present a time-dependent earthquake recurrence interval calculation because the time passed since the last large earthquake is not well constrained.

**Size dependency**: Based on the field mapping of block sizes and the expected block sizes which correspond both to the sizes of OSL dated blocks and the CRSP simulation block diameters (Table 1; Fig. 3), the probability of a given block size or smaller is predicted by Eq. (3). Considering the time dependent probability and the probabilities for given block sizes detailed above, the probability for rockfall hazard per specific block size ($H_R$) may be predicted as Eq. (5):

$$H_R = (1 - P_D) \cdot P_{EQ} \qquad (5)$$

where $P_D$ is the cumulative probability per block diameter D (Table 1) and $P_{EQ}$ is the rockfall occurrence probability calculated above to be 9%. Accordingly, predicted $H_R$ for the next 50 years for block diameters D between 2.7~~ and ~~6.2 m is ~~$H_R$~~ ~3% and for larger blocks~~ only~~, D between 4.6~~ and ~~6.2 m is ~~$H_R$~~ ~1%.~~ We do not present a time-dependent earthquake recurrence interval calculation because the time passed since the last large earthquake is not well constrained.~~

**Susceptibility:** As presented in Figures 8-9, the urban area and the area of open slopes above it subjected to rockfall hazard extends to about 1.55 km$^2$. We conclude that this area has a probability $H_R$ of ~1%-3% for impact by rockfall in the next 50 years.

## 6. Conclusions

In this work, we studied rockfall hazard for the town of Qiryat~~-~~Shemona (northern Israel) to demonstrate computer-simulation based hazard evaluation in cases where the study area is residing ~~below a cliff~~ in an ~~apriori~~a priori exposure to rockfall hazard, but no documentation of ~~recent or~~ past ~~rockfalls~~rockfall events is available. To overcome this lack of observations, we derived the needed geometrical and mechanical parameters for the computer hazard ~~analysis from field study of past events. We located areas subject to current rockfall hazard at the south-western quarters of town.~~modeling from a field study of downslope blocks. In particular, we analyzed the spatial distribution of individual rock-blocks which are the result of the past rockfalls and used this analysis for calibration of the model parameters.

OSL age determination of several past rockfall events in the study area suggests that these rockfalls were triggered by large (M>6) historical earthquakes, and in accordance, the estimated rockfall recurrence interval is hundreds of years. Nevertheless, we conclude that not all historical large earthquakes triggered rockfalls~~.~~ in the studied area. Additionally, we infer that the

downslope travel distance of the blocks is not significantly affected by the magnitude of seismic accelerations. However, earthquakes appear to play a significant role as the triggering mechanism of the rockfall. We found that falling blocks would come to a stop once the slope angle decreases to around 5°-10°.

The field ~~–~~calibrated simulation results ~~indicate that in~~indicated rockfall hazard at the ~~studied slope, falling blocks would stop after covering a distance~~south-western quarters of ~~several tens of meters once~~town as well as at the ~~slope angle decreases to around 5°-10°.~~slopes above the town. Considering the size distribution of the past rockfalls in the study area and the ~~reoccurrence~~recurrence time of large earthquakes in the area, the probability to be affected by a destructive rockfall within a 50 years time-window is ~~of~~ less than 5%.

## Acknowledgments

This work was funded by the National Steering Committee for Earthquake Preparedness in Israel. We wish to thank the Nature & National Parks Authority of Israel, allowing field-work at the Qiryat-Shemona National Park. MK wishes to thank Gal Hartman, Gaby Yelin, Shalev Siman-Tov and Yariv Nofech for their great help ~~during field work.~~ in field work. We thank two anonymous reviewers for their valuable comments and suggestions that significantly improved the manuscript. ~~This work was funded by the National Steering Committee for Earthquake Preparedness in Israel.~~

## References

Agliardi, F., and Crosta, G.B., 2003, High resolution three-dimensional numerical modelling of rockfalls: International Journal of Rock Mechanics and Mining Sciences, v. 40, p. 455-471.

Ambraseys, N.N., 1997, The earthquake of 1 January 1837 in Southern Lebanon and N orthern Israel. ~~PAGES?~~

Ambraseys, N.N., and Barazangi, M., 1989, The 1759 Earthquake in the Bekaa Valley: Implications for Earthquake Hazard Assessment in the Eastern Mediterranean Region: J. Geophys. Res., v. 94, p. 4007-4013.

Amiran, D.H.K., Arieh, E., and Turcotte, T., 1994, Earthquakes in Israel and Adjacent Areas - Macroseismic Observations since 100 Bce: Israel Exploration Journal, v. 44, p. 260-305.

Badoux, A., Andres, N., Techel, F., and Hegg, C.: Natural hazard fatalities in Switzerland from 1946 to 2015, 2016, Nat. Hazards Earth Syst. Sci., 16, 2747-2768, https://doi.org/10.5194/nhess-16-2747-2016.

Becker, A., and Davenport, C.A., 2003, Rockfalls triggered by the AD 1356 Basle Earthquake: Terra Nova, v. 15, p. 258-264.

Begin, Z.B., 2005, Destructive earthquakes in the Jordan Valley and the Dead Sea — their reoccurrence interval and the probability of their occurrence, Geol. Surv. Israel, Report GSI/12/2005.

Ben-Menahem, A., 1991, Four Thousand Years of Seismicity Along the Dead Sea Rift: J. Geophys. Res., v. 96. no. B12, p. 20195-20216.

Brunetti, M.T., Guzzetti, F., and Rossi, M., 2009, Probability distributions of landslide volumes: Nonlin. Processes Geophys., v. 16, p. 179-188.

Crosta, G.B., and Agliardi, F., 2004, Parametric evaluation of 3D dispersion of rockfall trajectories: Natural Hazards and Earth System Sciences, v. 4, p. 583-598.

Cruden, D.M., and Varnes, D.J., 1996, Landslide Types and Processes, *in* Turner, A., and Schuster, R., eds., Landslides-Investigation and Mitigation. Transportation Research Board Special Report 247, National Research Council, USA, p. 36–75.

Daëron, M., Klinger, Y., Tapponnier, P., Elias, A., Jacques, E. and Sursock, A., 2007, 12,000-Year-Long Record of 10 to 13 Paleoearthquakes on the Yammoûneh Fault, Levant Fault System, Lebanon. Bulletin of the Seismological Society of America, 97 (3). pp. 749-771.

D'Amato, J., Hantz, D., Guerin, A., Jaboyedoff, M., Baillet, L., and Mariscal, A., 2016, Influence of meteorological factors on rockfall occurrence in a middle mountain limestone cliff, Nat. Hazards Earth Syst. Sci., 16, 719-735, https://doi.org/10.5194/nhess-16-719-2016.

De Biagi, V., Napoli, M. L., Barbero, M., and Peila, D., 2017, Estimation of the return period of rockfall blocks according to their size, Nat. Hazards Earth Syst. Sci., 17, 103-113, https://doi.org/10.5194/nhess-17-103-2017.

Dorren, L.K.A., 2003, A review of rockfall mechanics and modelling approaches: Progress in Physical Geography, v. 27, p. 69-87.

Dussauge-Peisser, C., Helmstetter, A., Grasso, J.R., Hantz, D., Desvarreux, P., Jeannin, M., and Giraud, A., 2002, Probabilistic approach to rock fall hazard assessment: potential of historical data analysis: Natural Hazards and Earth System Sciences, v. 2, p. 15-26.

Dussauge, C., Grasso, J.R., and Helmstetter, A.S., 2003, Statistical analysis of rockfall volume distributions: Implications for rockfall dynamics: Journal of Geophysical Research-Solid Earth, v. 108. no. B6.

Elias, A., Tapponnier, P., Singh, S.C., King, G.C.P., Briais, A., Daeron, M., Carton, H., Sursock, A., Jacques, E., Jomaa, R., and Klinger, Y., 2007, Active thrusting offshore Mount Lebanon: Source of the tsunamigenic A.D. 551 Beirut-Tripoli earthquake: Geology, v. 35, p. 755-758.

Evans, S.G., 1997, Fatal landslides and landslide risk in Canada, *in* Cruden, D.M., and Fell, R., eds., Inter. Workshop on Landslide Risk Assessment: Honolulu, p. 185-196.

Evans, S.G., and Hungr, O., 1993, The assessment of rockfall hazard at the base of talus slopes: Canadian Geotechnical Journal, v. 30, p. 620-636.

Flageollet, J.C., and Weber, D., 1996, Fall, *in* Dikau, R., and others, eds., Landslide recognition, identification, movement and causes: New York, Wiley, p. 13–28.

Freund, R., 1965, A model of the structural development of Israel and adjacent areas since upper Cretaceous times: Geological Magazine, v. 102, p. 189-205.

Garfunkel, Z., 1981, Internal structure of the dead-sea leaky transform (rift) in relation to plate kinematics: Tectonophysics, v. 80, p. 81-108.

Giani, G.P., Giacomini, A., Migliazza, M., and Segalini, A., 2004, Experimental and Theoretical Studies to Improve Rock Fall Analysis and Protection Work Design: Rock Mechanics and Rock Engineering, v. 37, p. 369-389.

Glikson, Y.A., 1966, Geology of southern Naftali Mountains (northeastern Galilee, Israel): Isr. J. Earth Sci., v. 15, p. 135-154.

Guidoboni, E., and Comastri, A., 2005, Catalogue of earthquakes and tsunamis in the Mediterranean area from the 11th to the 15th century: Roma, Instituto Nazionale di Geofisica e Vulcanologia, 1037 p.

Guidoboni, E., Comastri, A., and Traina, G., 1994, Catalogues of Ancient Earthquakes in the Mediterranean Area up to the 10th Century: Roma, Instituto Nazionale di Geofisica e Vulcanologia, 504 p.

Guzzetti, F., 2000, Landslide fatalities and the evaluation of landslide risk in Italy: Engineering Geology, v. 58, p. 89-107.

Guzzetti, F., Crosta, G., Detti, R., and Agliardi, F., 2002, STONE: a computer program for the three-dimensional simulation of rock-falls: Computers & Geosciences, v. 28, p. 1079-1093.

Guzzetti, F., Reichenbach, P., Cardinali, M., Galli, M., and Ardizzone, F., 2005, Probabilistic landslide hazard assessment at the basin scale: Geomorphology, v. 72, p. 272-299.

Guzzetti, F., Reichenbach, P., and Ghigi, S., 2004, Rockfall Hazard and Risk Assessment Along a Transportation Corridor in the Nera Valley, Central Italy: Environmental Management, v. 34, p. 191-208.

Guzzetti, F., Reichenbach, P., and Wieczorek, G.F., 2003, Rockfall hazard and risk assessment in the Yosemite Valley, California, USA: Natural Hazards and Earth System Sciences, v. 3, p. 491-503.

Hamiel, Y., Amit, R., Begin, Z.B., Marco, S., Katz, O., Salamon, A., Zilberman, E., and Porat, N., 2009, The Seismicity along the Dead Sea Fault during the Last 60,000 Years: ~~Bulletin~~Bull. of the Seismological Society of America, v. 99, p. 2020-2026.

IMS, 2007, IMS website: Climate information - long term info Volume http://www.ims.gov.il/IMSEng/CLIMATE/LongTermInfo/, Israel Meteorological Service.

Jones, C.L., Higgins, J.D., and Andrew, R.D., 2000, Colorado Rockfall Simulation Program Version 4.0 Manual, Colorado Department of Transportation, Denver, CO 80222.

Kafri, U., 1991, Lithostratigraphy of Judea Group in eastern Galilee, emphasizing the Naftali Mountains. Geological Survey of Israel, GSI/24/91.

Kagan, E.J., Agnon, A., Bar-Matthews, M., and Ayalon, A., 2005, Dating large infrequent earthquakes by damaged cave deposits. Geology, v. 33, p. 261-264.

Kanari, M., 2008, Evaluation of rockfall hazard to Qiryat-Shemona - possible correlation to earthquakes: Jerusalem, Geological Survey of Israel, report GSI /24/2008, 115 pp.

Kanari, M., Katz, O., Porat, N., Weinberger, R., and Marco, S., 2008, Evaluation of rockfall hazard and risk to a town within the Dead Sea fault zone (Qiryat-Shemona, northern Israel). Geophysical Research Abstracts, Vol. 10, EGU2008-A-05592, EGU General Assembly 2008, Volume 10.

Katz, O., and Aharonov, E., 2006, Landslides in vibrating sand box: What controls types of slope failure and frequency magnitude relations? Earth and Planetary Science Letters, v. 247, p. 280-294.

Katz, O., and Crouvi, O., 2007, The geotechnical effects of long human habitation (2000< years): Earthquake induced landslide hazard in the city of Zefat, northern Israel: Engineering Geology, v. 95, p. 57-78.

Katz, O., Amit, R., Yagoda-Biran, G., Hatzor, Y. H., 2010, Quaternary earthquakes and landslides in the Sea of Galilee area, the Dead Sea Transform; paleoseismic analysis and evaluation of current hazard. Isr. J. Earth Sci., 58: 275-294.

Katz, O., Reichenbach, P., and Guzzetti, F., 2011, Rock fall hazard along the railway corridor to Jerusalem, Israel, in the Soreq and Refaim valleys: Natural Hazards, v. 56, p. 649-665.

Keefer, D.K., 1984, Landslides caused by earthquakes: Geological Society of America Bulletin, v. 95, p. 406-421.

Keefer, D.K., 2002, Investigating Landslides Caused by Earthquakes – A Historical Review: Surveys in Geophysics, v. 23, p. 473-510.

Kobayashi, Y., Harp, E.L. and Kagawa, T., 1990. Simulation of rockfalls triggered by earthquakes. Rock Mechanics and Rock Engineering, 23(1): 1-20.

Lian, O.B., and Roberts, R.G., 2006, Dating the Quaternary : progress in luminescence dating of sediments: Quaternary Science Reviews, v. 25, p. 2449-2468.

Mackey, B. H., and Quigley, M. C., 2014, Strong proximal earthquakes revealed by cosmogenic 3He dating of prehistoric rockfalls, Christchurch, New Zealand: Geology, v. 42, no. 11, p. 975-978.

Malamud, B.D., Turcotte, D.L., Guzzetti, F., and Reichenbach, P., 2004, Landslide inventories and their statistical properties: Earth Surface Processes and Landforms, v. 29, p. 687-711.

Marco, S., Agnon, A., Ellenblum, R., Eidelman, A., Basson, U., and Boas, A., 1997, 817-year-old walls offset sinistrally 2.1 m by the Dead Sea Transform, Israel: Journal of Geodynamics, v. 24, p. 11-20.

Marco, S., Hartal, M., Hazan, N., Lev, L., and Stein, M., 2003, Archaeology, history, and geology of the A.D. 749 earthquake, Dead Sea transform: Geology, v. 31, p. 665-668.

Marco, S., Rockwell, T.K., Heimann, A., Frieslander, U., and Agnon, A., 2005, Late Holocene activity of the Dead Sea Transform revealed in 3D palaeoseismic trenches on the Jordan Gorge segment: Earth and Planetary Science Letters, v. 234, p. 189-205.

Marco, S., Stein, M., Agnon, A., and Ron, H., 1996, Long-term earthquake clustering: A 50,000-year paleoseismic record in the Dead Sea Graben: Journal of Geophysical Research-Solid Earth, v. 101, p. 6179-6191.

Matmon, A., Shaked, Y., Porat, N., Enzel, Y., Finkel, R., Lifton, N., Boaretto, E., and Agnon, A., 2005, Landscape development in an hyperarid sandstone environment along the margins of the Dead Sea fault: Implications from dated rock falls: Earth and Planetary Science Letters, v. 240, no. 3, p. 803-817.

Migowski, C., Agnon, A., Bookman, R., Negendank, J.F.W., and Stein, M., 2004, Recurrence pattern of Holocene earthquakes along the Dead Sea transform revealed by varve-counting and radiocarbon dating of lacustrine sediments: Earth and Planetary Science Letters, v. 222, p. 301-314.

Nemer, T., and Meghraoui, M., 2006, Evidence of coseismic ruptures along the Roum fault (Lebanon): a possible source for the AD 1837 earthquake: Journal of Structural Geology, v. 28, p. 1483-1495.

Pellicani, R., Spilotro, G., and Van Westen, C. J., 2016, Rockfall trajectory modeling combined with heuristic analysis for assessing the rockfall hazard along the Maratea SS18 coastal road (Basilicata, Southern Italy): Landslides, v. 13, no. 5, p. 985-1003.

Pfeiffer, T.J., and Bowen, T., 1989, Computer simulation of rockfalls: Bulletin of the Association of Engineering Geologists, v. 26, p. 135-146.

Quennell, A.M., 1958, The Structural and geomorphic evolution of the Dead Sea Rift: Quarterly Journal of the Geological Society, v. 114, p. 1-24.

Ritchie, A.M., 1963, The evaluation of rock fall and its control: Highway Research Record, p. 13-28.

Rinat, Y., Matmon, A., Arnold, M., Aumaître, G., Bourlès, D., Keddadouche, K., Porat, N., Morin, E., and Finkel, R. C., 2014, Holocene rockfalls in the southern Negev Desert, Israel and their relation to Dead Sea fault earthquakes: Quaternary Research, v. 81, no. 2, p. 260-273.

Scholz, C.H., 2002, The Mechanics of Earthquakes and Faulting: New York, Cambridge Univ. Press, 471 p.

Shapira, A. (ed.), 2002, An updated map of peak ground accelerations for Israeli Standard 413, *in* http://www.gii.co.il/heb/Teken/report_413.htm.

Shtober-Zisu, N., 2006, Quaternary tectonic geomorphology along the Naftali Mountain front [PhD thesis]: Tel Aviv, Tel Aviv University.

Siman-Tov, S., 2009, The Geomorphic and Mechanical Conditions for Rock-Falls: Rama Cliff, Zurim Escarpment. M.Sc thesis (In Hebrew, abstract in English): Jerusalem, The Hebrew University. 85pp.

Siman-Tov, S., Katz, O., and Matmon, A., 2017, Examining the effects of ground motion and rock strength on the size of boulders falling from an overhanging cliff: Engineering Geology, v. 220, p. 164-174.

Sneh, A., and Weinberger, R., 2003a, Geology of the Metulla quadrangle 1:50,000: Implications for the stratigraphic division and the fault system around the Hula Valley: Jerusalem, Geological Survey of Israel.

Sneh, A., and Weinberger, R. 2003b. Geology of the Metulla quadrangle, northern Israel: Implications for the offset along the Dead Sea Rift, Isr. J. Earth Sci., 52:123-138.

Strunden, J., Ehlers, T. A., Brehm, D., and Nettesheim, M., 2015, Spatial and temporal variations in rockfall determined from TLS measurements in a deglaciated valley, Switzerland: Journal of Geophysical Research: Earth Surface, v. 120, no. 7, p. 1251-1273.

Times of Israel, 14-Jan-2019, Towns flood in north as forecasts see cold snap; snow in Jerusalem, https://www.timesofisrael.com/towns-flood-in-north-as-forecasts-see-cold-snap-snows-later-this-week.

Varnes, D.J., 1978, Slope movement types and processes, *in* Schuster, R.L., and Krizek, R.J., eds., Landslides, analysis and control, Volume Special Report 176: Washington, D.C., Transportation Research Board, National Research Council, p. 11-33.

Vidrih, R., Ribicic, M. and Suhadolc, P., 2001. Seismogeological effects on rocks during the 12 April 1998 upper Soca Territory earthquake (NW Slovenia). Tectonophysics, 330: 153-175.

Wechsler, N., Katz, O., Dray, Y., Gonen, I., and Marco, S., 2009, Estimating location and size of historical earthquake by combining archaeology and geology in Umm-El-Qanatir, Dead Sea Transform: Natural Hazards, v. 50, p. 27-43.

Wechsler, N., Rockwell, T. K., Klinger, Y., Štěpančíková, P., Kanari, M., Marco, S., and Agnon, A., 2014, A Paleoseismic Record of Earthquakes for the Dead Sea Transform Fault between the First and Seventh Centuries C.E.: Nonperiodic Behavior of a Plate Boundary Fault. Bulletin of the Seismological Society of America. doi: 10.1785/0120130304.

Wei, L.-W., Chen, H., Lee, C.F., Huang, W.-K., Lin, M.-L., Chi, C.-C., and Lin, H.-H., 2014, The mechanism of rockfall disaster: A case study from Badouzih, Keelung, in northern Taiwan: Engineering Geology, v. 183, p. 116-126.

Weinberger, R., Gross, M.R. and Sneh, A. 2009. Evolving deformation along a transform plate boundary: example from the Dead Sea Fault in northern Israel, Tectonics, 28, TC5005, doi:10.1029/2008TC002316.

Whalley, W.B., 1984, Rockfalls, *in* Brunsden, D., and Prior, D., eds., Slope Stability: New York, Wiley, p. 217–256.

Wieczorek, G.F. and Jäger, S., 1996. Triggering mechanisms and depositional rates of postglacial slope-movement processes in the Yosemite Valley, California. Geomorphology, 15: 17-31.

Wintle, A. G. & Murray, A. S. 2006. A review of quartz optically stimulated luminescence characteristics and their relevance in single-aliquot regeneration dating protocols. Radiation Measurements, 41(4), 369–391.

Wintle, A.G. 2008. Fifty years of luminescence dating. Archaeometry 50, 276-312.

Yagoda-Biran, G., Hatzor, Y.H., Amit, R., and Katz, O., 2010, Constraining regional paleo peak ground acceleration from back analysis of prehistoric landslides: Example from Sea of Galilee, Dead Sea transform: Tectonophysics, v. 490, p. 81-92.

## Tables

**Table 1. Size distribution of the mapped rock blocks (N=76)**

| Volume bin ($m^3$) | Diameter (m)* | Cumulative frequency* | predicted cumulative Probability $P_D$** |
|---|---|---|---|
| 1 | 1.3 | - | - |
| 10 | 2.7 | 50 | 0.67 |
| 50 | 4.6 | 71 | 0.89 |

| | | | |
|---|---|---|---|
| 100 | 5.8 | 74 | 0.99 |
| 125 | 6.2 | 76 | 1 |

* No data collected for blocks smaller than 1 $m^3$. (cumulative frequency is zero).

** $P_D$ is calculated using Eq. [3] for a given block diameter or smaller.

**Table 2. Predicted velocity (m/s) and kinetic energy (kJ) of falling blocks at town border***

| D (m) | 1.3 | | 2.7 | | 4.6 | | 5.8 | | 6.2 | |
|---|---|---|---|---|---|---|---|---|---|---|
| **Profile** | **Vel** | **$E_K$** | **Vel** | **$E_K$** | **Vel** | **$E_K$** | **Vel** | **$E_K$** | **Vel** | **$E_K$** |
| 14 | 12.3 | 290 | 10.8 | 1,950 | 12.1 | 12,400 | 11.7 | 23,000 | 12.3 | 28,500 |
| 13 | 12.5 | 310 | 12.2 | 2,600 | 12.6 | 13,900 | 12.4 | 27,100 | 12.6 | 34,000 |
| 12 | 11.1 | 240 | 10.0 | 1,700 | 11.7 | 11,500 | 11.3 | 22,000 | 11.4 | 27,500 |
| 11 | 12.4 | 295 | 11.5 | 2,300 | 12.0 | 12,300 | 12.7 | 27,300 | 12.7 | 34,000 |
| 10 | 9.3 | 165 | 8.3 | 1,200 | 9.5 | 7,400 | 9.3 | 14,600 | 9.3 | 19,000 |
| 8 | 10.5 | 220 | 11.3 | 2,200 | 11.5 | 11,400 | 11.6 | 22,900 | 13.8 | 40,300 |
| 9 | n/a | n/a | 13.0 | 2,950 | 13.7 | 16,300 | 13.8 | 32,300 | 11.7 | 29,000 |

* Values presented are maximal simulated velocity (Vel) and kinetic energy ($E_k$) per rock diameter (D). Profiles listed (7 out of total 25 simulated profiles) are only those which are predicted to impact town border. Analysis points located at distances along slope which are equal or up to 50 m shorter than the town border. See text for detail.

**Table 3. OSL age field and laboratory data, with age determination results.**

| Sample* | Block No. | Depth (m) | γ+cosm. (μGy/a) | K (%) | U (ppm) | Th (ppm) | Ext. α (μGy/a) | Ext. β (μGy/a) | Total dose (μGy/a) | No. of discs | OD (%) | De (Gy) | Age (ka) |
|---|---|---|---|---|---|---|---|---|---|---|---|---|---|
| QS-1 | 015 | 1.2 | 945 | 0.80 | 1.3 | 6.0 | 7 | 745 | 1697±102 | 21/22 | 12±1.836 | 15±2 | 8.7.0±1.10 |
| QS-3 | 008 | 0.7 | 762 | 1.0 | 2.0 | 8.4 | 10 | 995 | 1767±94 | 20/21 | 25 | 2.79±0.21 | 1.56±0.131 |
| QS-4 | 010 | 0.6 | 577 | 1.0 | 1.6 | 6.6 | 8 | 910 | 1495±77 | 21/24 | 51 | 1.56±0.31 | 1.0.89±0.161 |
| QS-5 | 007 | 0.5 | 744 | 0.76 | 1.3 | 4.0 | 6 | 680 | 1429±85 | 25/25 | 29 | 5.74±0.93 | 4.3.8±0±0.7.3 |
| QS-6 | 064 | 0.4 | 554 | 0.46 | 1.3 | 4.9 | 6 | 520 | 1080±64 | 22/25 | 42 | 2.3±0.51 | 2.21±0.502 |
| QS-9 | 013 | 0.3 | 455 | 0.65 | 1.6 | 7.1 | 8 | 712 | 1175±62 | 24/25 | 62 | 5.0±0.6 | 4.3±0.6±1.4 |
| QS-11 | 016 | 0.3 | 536 | 0.58 | 1.7 | 6.3 | 8 | 665 | 1209±67 | 22/23 | 60 | 2.71±0.93 | 2.21.7±0.72 |
| QS-12 | 036 | 1.2 | 905 | 1.08 | 1.9 | 9.0 | 10 | 1041 | 1256±108 | 23/25 | 38 | 8.8±0±1.7.6 | 4.15±0.94 |
| QS-13 | 017 | 0.4 | 486 | 1.05 | 1.8 | 8.6 | 10 | 1003 | 1481±73 | 24/25 | 53 | 4.7±0.5 | 3.2±0.4 |

* Quartz grainGrain size extracted for all samples wasis 74-125 μm, except for samples QS-1 and QS-2, for which grain size 88-125 μm was used. Water moisture estimated at 15±5%. The quartz was etched by concentrated HF for 40 minutes.

**Table 4. Selected historic earthquakes, candidates as possible rockfall triggers in the ~~studied~~study area***

| Date | Age | Max estimated local int./~~mag~~Mag. | age cluster | OSL samples |
|---|---|---|---|---|
| 1202 AD | 0.81 ka | IX | ~~0.9 ±0.17 ka~~ no-fit | ~~QS-4~~ |
| 1033 AD | 0.97 ka | IX-X | 1.0 ±0.1 ka | QS-4 |
| 749 AD | 1.26 ka | X | no-fit | |
| 659 AD | 1.35 ka | IX | no-fit | ~~QS-3~~ |
| 551 AD | 1.46 ka | VIII-IX | ~~1.5 ±0.15 ka~~ | QS-3 |
| 502 AD | 1.51 ka | X | 1.7 ±0.25 ka | QS-3, QS-11 |
| 363 AD | 1.64 ka | IX | ~~no fit~~ | QS-3, QS-11 |
| 199 BC | 2.21 ka | X | 2.2 ±0.60 ka | QS-6~~, QS-9, QS-11~~ |
| 759 BC | 2.77 ka | - (M 7.3) | 3.2 ±0.45 ka | QS-~~9, QS-11~~13 |
| 2050-2100 BC | Ca. 4.2 ka | M 6.8-8.0 | 4.3 ±0~~±0.2~~.6 ka | QS-5, QS-9, QS-12~~(QS-9)~~ |
| n/a | Ca. ~~6~~9 ka | M 7.0 | 8.7~~.0~~ ±1.0 ka | QS-1 |

* A list of candidate rockfall triggering earthquakes, which contains historical earthquakes that: (a) occurred within the time spans of the OSL ages; (b) maximum estimated intensity is at least 'IX' on an EMS macroseismic local intensity scale and/or their estimated moment-magnitude from previous paleoseismic studies is 6 or larger; (c) the distance between the study area and affected localities reported does not exceed 100 km (following Keefer, 1984).

## Figure Captions

**Figure 1 (a)** Location map of the study area on the backdrop of major ~~faults~~fault segments of the DST~~;~~ (Ro=Roum, Y=Yammuneh, H=Hatsbaya, Ra=Rashaya; S=Serghaya); Inset shows the plate tectonic setting of the DST**; (b)** Orthophoto map of the study area (black rectangle). The rockfall source, Ein-El-Assad Formation (EEA), is marked by a blue line; town border in red dashed line.

**Figure 2** ~~A block at its stop site and the~~ The source for rockfalls~~:~~, the cliff of Ein El Assad Formation, at the back~~. The~~ and a rock-block at its stop site. This large boulder, ~41 $m^3$, is block no 016 (Table 3), under which ~~OSL~~ sample QS-11 for OSL age determination was excavated.

**Figure 3** ~~Block mapping areas: green outline - field mapping~~Map of fallen rock-blocks in the studied area~~, where~~. Green squares are 76 blocks ~~>1 m3 (green squares) were~~ mapped in the field within the area marked by green outline; these blocks were used to calculate the block volume distribution (PDF) detailed in Fig. 6; Yellow squares are 200 blocks mapped using aerial photos within the area marked by black rectangle; blocks sampled for OSL age determination are marked in red circles~~; black rectangle outline - area where blocks were mapped from 1946 and 1951 aerial photos (blocks in yellow squares).~~ Size of squares denotes block diameter bins, see legend. Pink lines represent slope profiles on which CRSP calibration simulations were run.

**Figure 4** Location of 25 simulation profiles of rockfall trajectories. Faults traces are from Sneh and Weinberger (2003a). The source for the rock-falls (Ein-el-Assad formation) is marked with blue line.

**Figure 5** Field observed distance from the source and maximal simulated travel distances of rock blocks. Block diameters are both size- and color-coded. The 1:1 line (x=y) is plotted in gray.

**Figure 6** Probability density function (PDF) of field measured, D >1 $m^3$, block volumes (N=76).

**Figure 7 (a)** Schematic illustration of the CRSP modelled slope cells and explanation of the terms 'x% stop angle' (e.g. 50% stop angle is the angle of the slope cell where 50% of the blocks stop) and 'stop swath' (the farthest distance along the slope where 100% of the blocks stop). **(b)** Slope gradients of slope cells and gradients at ~~different~~ stop angles. Tangential ~~denotes~~ axes (X and Y axes) denote simulated profile ~~number~~numbers 1 to 25. Radial ~~denoted~~axis denotes the slope angles. Gradients for all cells per profile are plotted on an arc between 0 and 90 ~~of all cells along the profile. For example: the cells along profile 20 have slope angles that vary between 8°-36°,~~degrees: Red circles are 100% stop angles (slope angle of the profile cell at which cumulated 100% of simulated blocks stop); blue triangles are 50% stop angles; gray circles are all other cells in ~~each profile.~~the profile. For example: the cells along profile 16 have slope angles that vary between 8°-36°; the 100% stop angle is 11° (red circle) and the 50% stop angle is 8° (blue triangle). The red line represents the mean of all 100% stop angles for all profiles at 7.7° and the thick black lines represent its SD of 2.3°.

**Figure 8** Rockfall hazard map of the study area. The area subject to rockfall hazard is defined from the source escarpment to 100% stop line. Map compiled from maximal travel distance of 25 rockfall simulation profiles performed using CRSP (green lines in Fig. 4).

**Figure 9** Rockfall hazard map for the town of Qiryat Shemona. Yellow line represents the CRSP 100% stop line calculated for large blocks (D is 5.8 m and 6.2 m). Yellow-black hazard triangles mark simulated stop line and town border impact location for each profile; Orange-black hazard triangles mark simulated ~~stop line and~~ town border impact location for each profile; profile numbers in yellow refer to simulated profile numbers; indices with sword label '†' mark locations of rockfall impact at town border~~; inset: black rectangle outlines enlarged map area~~. Map location is shown on the inset.

**Figure 10** Summary of OSL ages ~~plotted in rank order and suggested rockfall triggering earthquakes. OSL age results for the past 8000 years in~~ (black circles with error bars~~;~~) plotted in chronological order and selected historical earthquakes suggested as rockfall triggers ~~using data from earthquake catalogs and paleoseismic data in~~(shown as vertical gray lines, chronologically labeled at top axis~~;~~); see text for details.

**Figure 11** Clustering of ~~OSL ages around historical earthquake dates. Five 'successes' for~~ rockfall events using binomial non-random temporal distribution ~~test defined~~ using a ±50 years time- window ~~(see text for detail); vertical lines are ±50 years time-window around earthquake dates (red solid lines and blue dashed lines are used to distinct between overlapping time windows; black circles are~~. Dated OSL rockfall ages marked in black circles by their central OSL ages with ±50 years black error bars ~~(black)~~ and their lab reported error ~~range (gray).~~ ranges in light-blue bars. Historical earthquake dates are marked on top axis and plotted with ±50 years time window (red stripes bounded by red solid lines represent time windows). See text for details about binomial distribution results and usage.

**Figures**

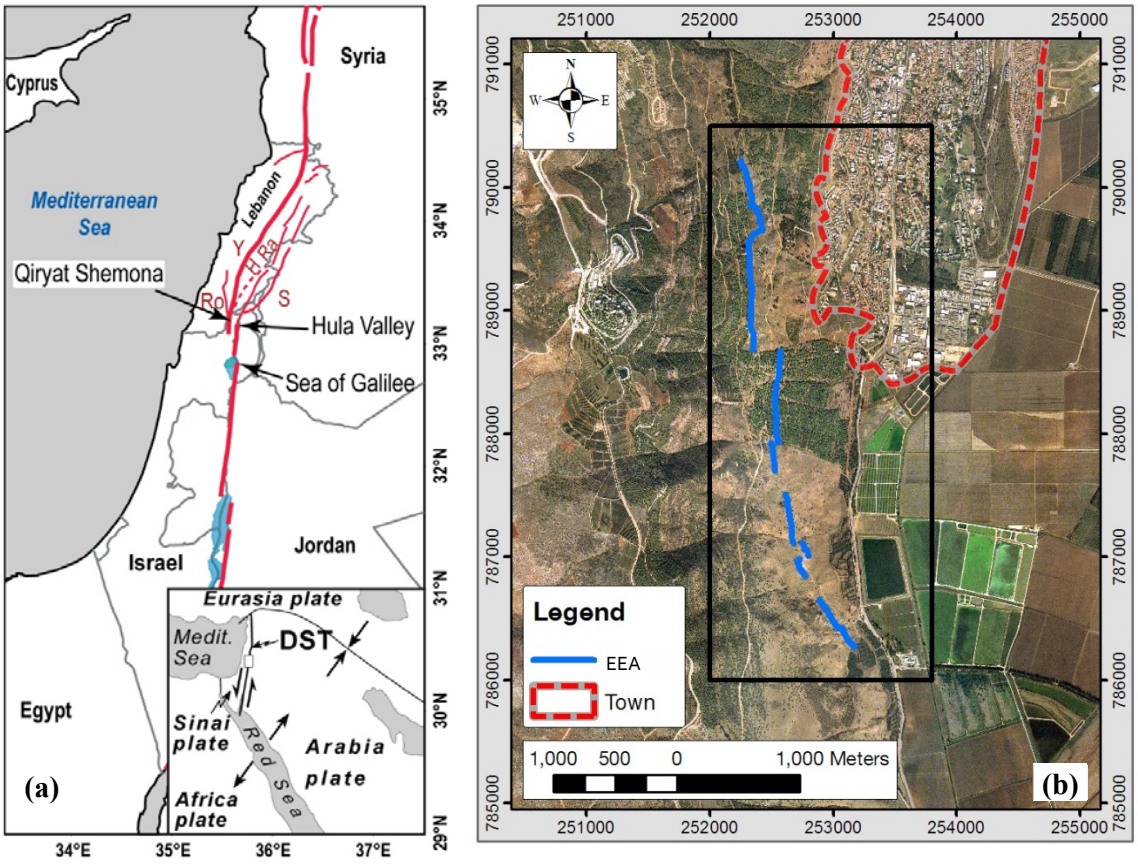


Fig. 1

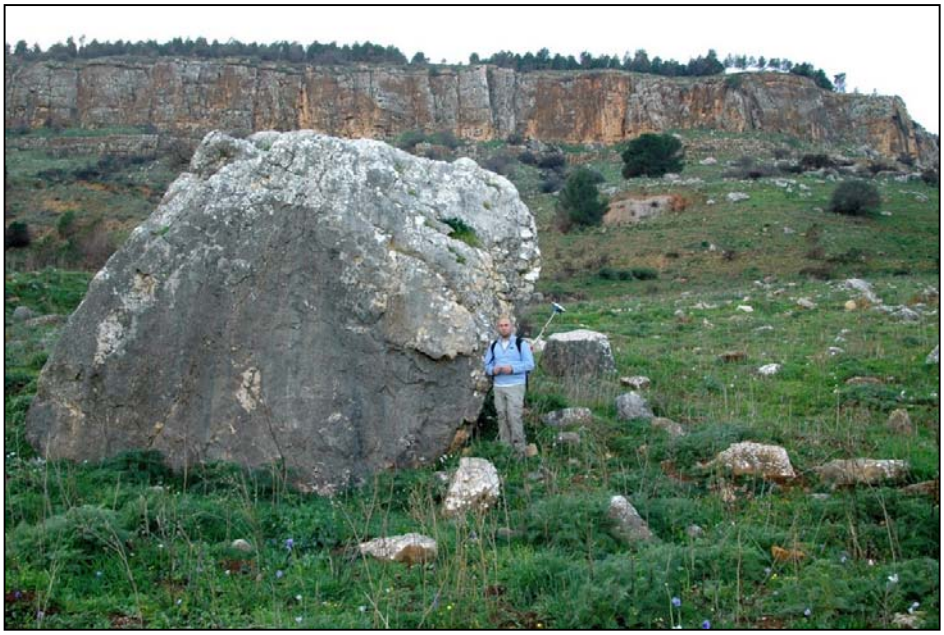

Fig. 2

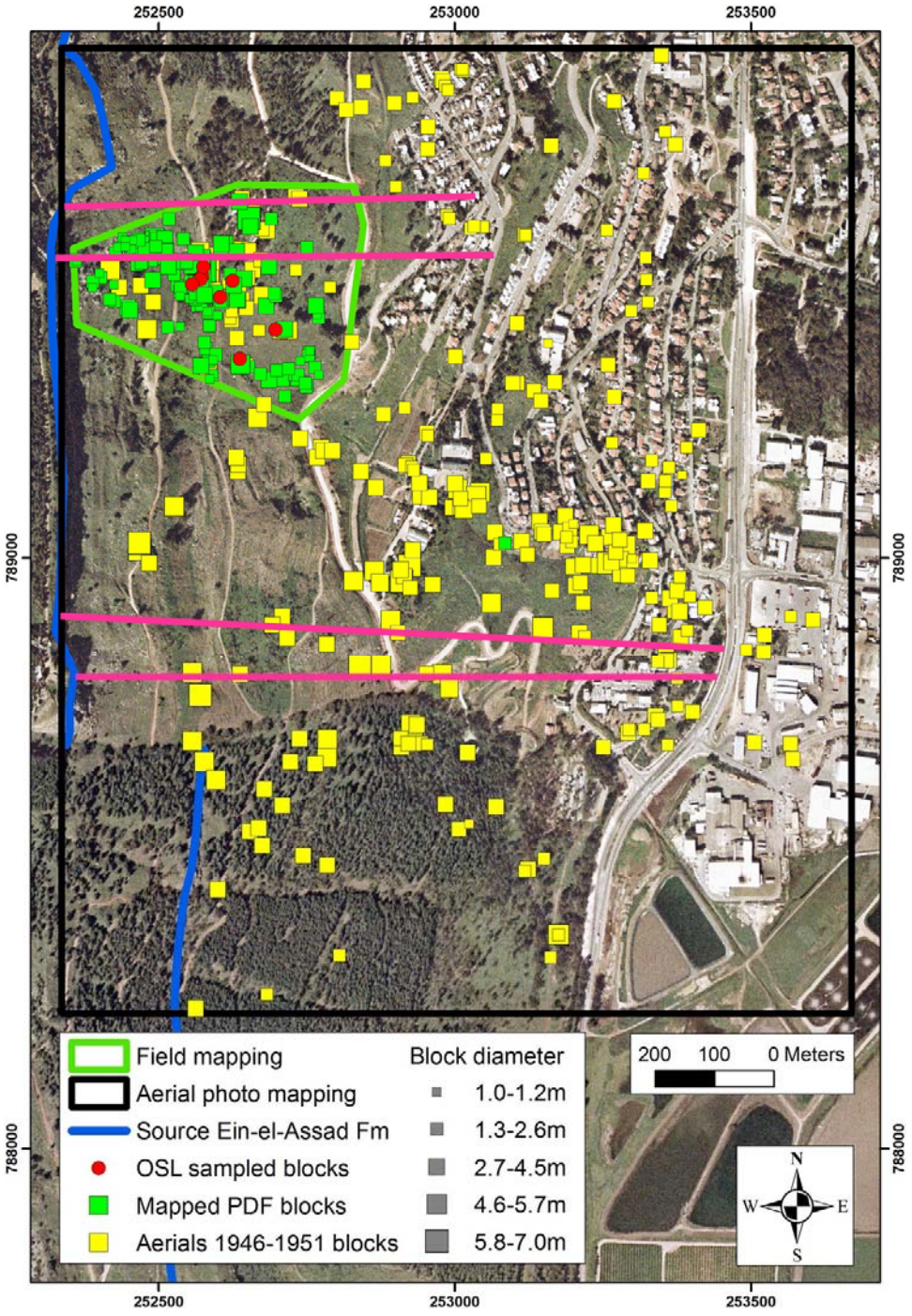
252500
253000
253500
789000
788000
Field mapping
Aerial photo mapping
Source Ein-el-Assad Fm
OSL sampled blocks
Mapped PDF blocks
Aerials 1946-1951 blocks
Block diameter
1.0-1.2m
1.3-2.6m
2.7-4.5m
4.6-5.7m
5.8-7.0m
200 100 0 Meters
N
W
E
S

Fig. 3

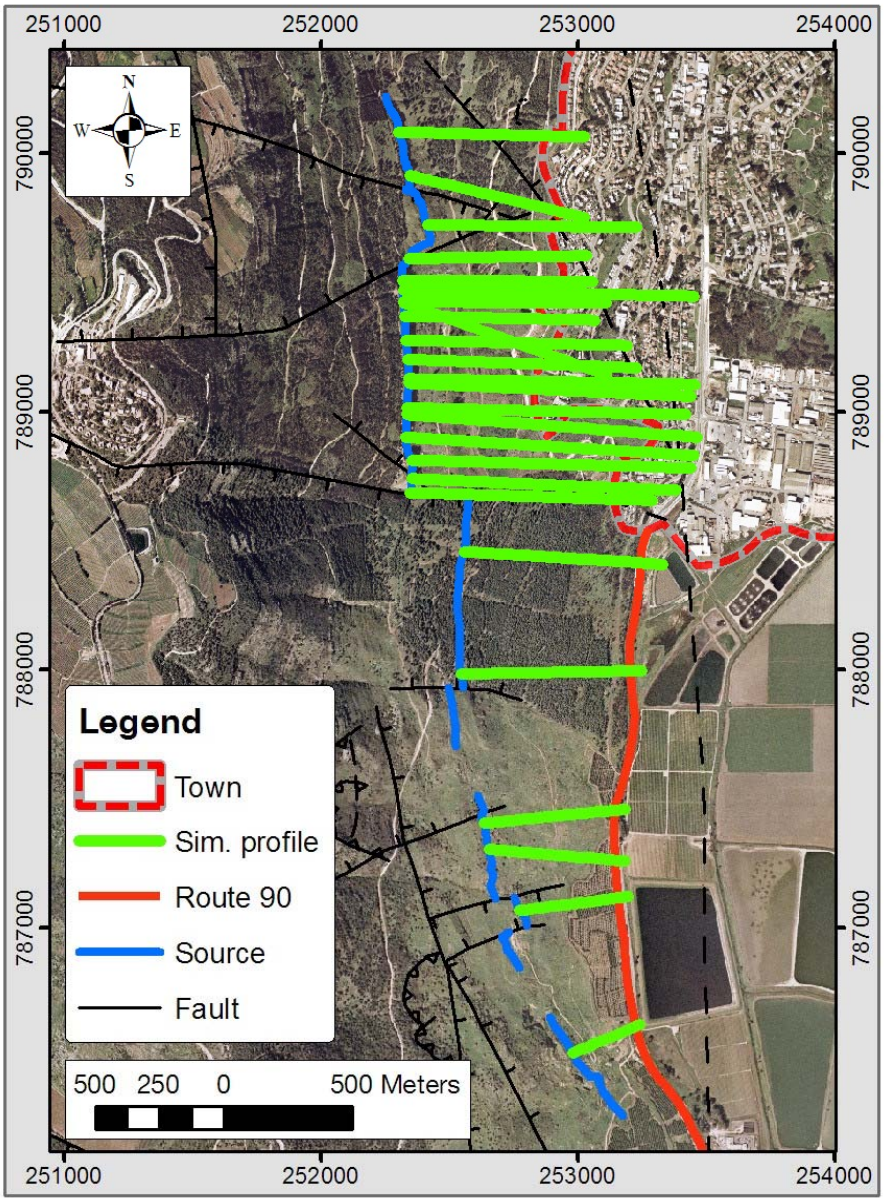
251000
252000
253000
254000
790000
789000
788000
787000
N
W
E
S
Legend
Town
Sim. profile
Route 90
Source
Fault
500 250 0 500 Meters

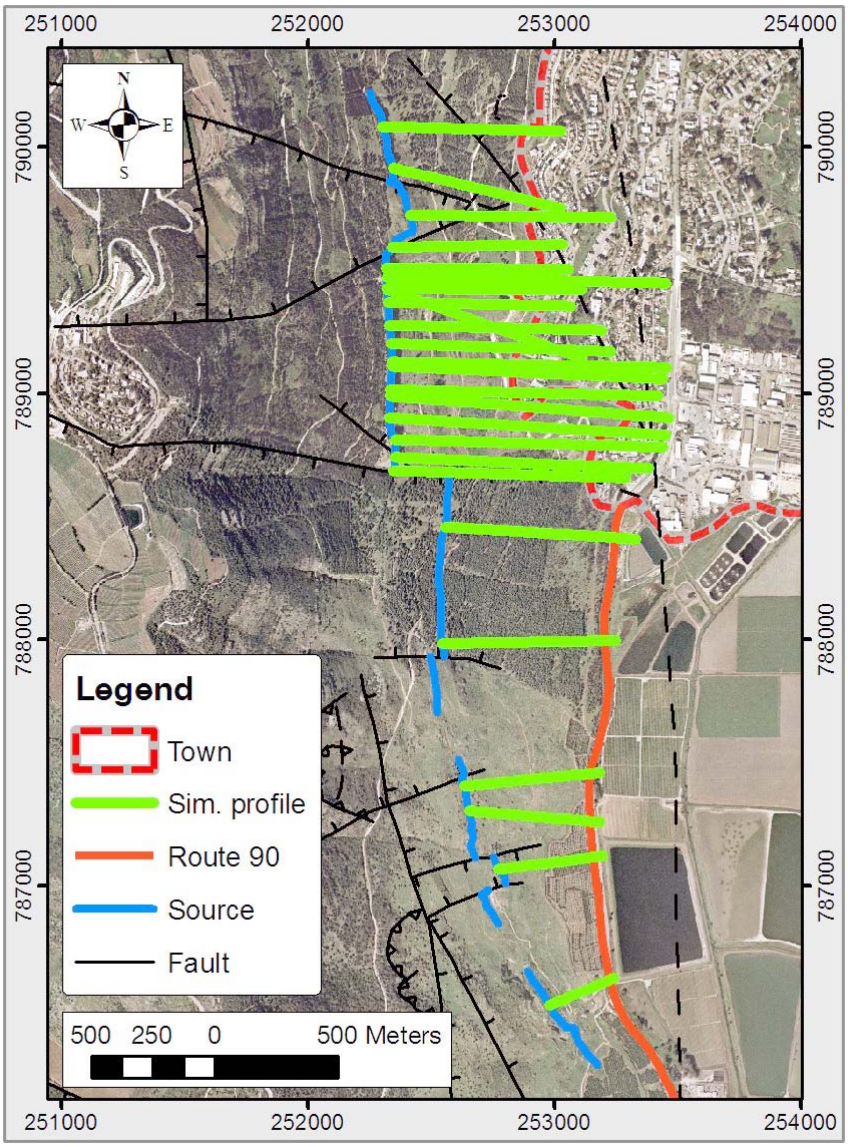
251000
252000
253000
254000
790000
789000
788000
787000
N
W
E
S
Legend
Town
Sim. profile
Route 90
Source
Fault
500 250 0 500 Meters

Fig. 4

5

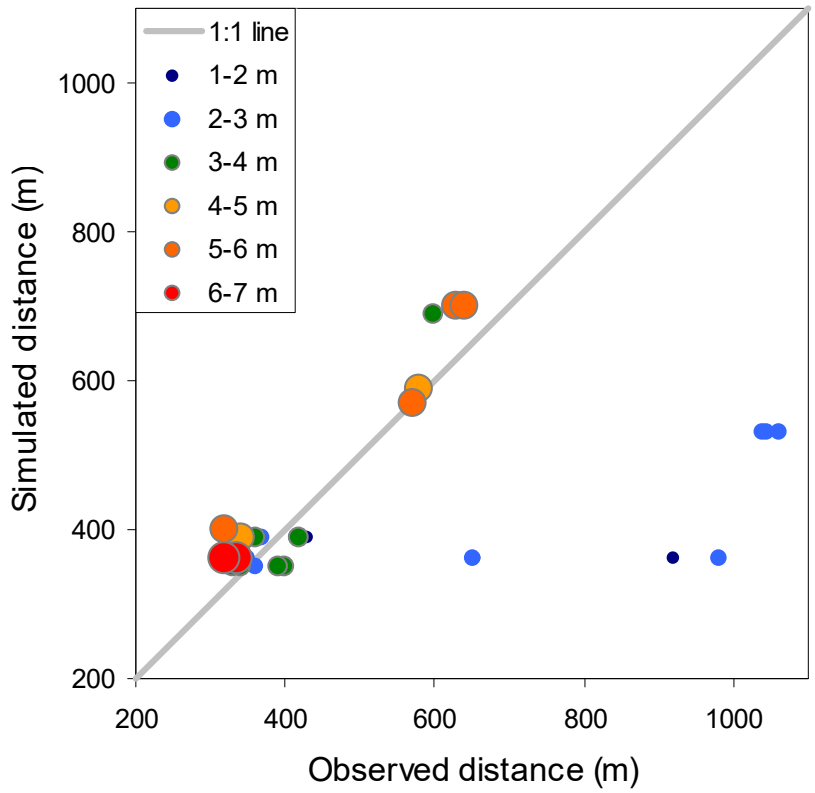
1:1 line
1-2 m
2-3 m
3-4 m
4-5 m
5-6 m
6-7 m
Simulated distance (m)
Observed distance (m)
200
400
600
800
1000

Fig. 5

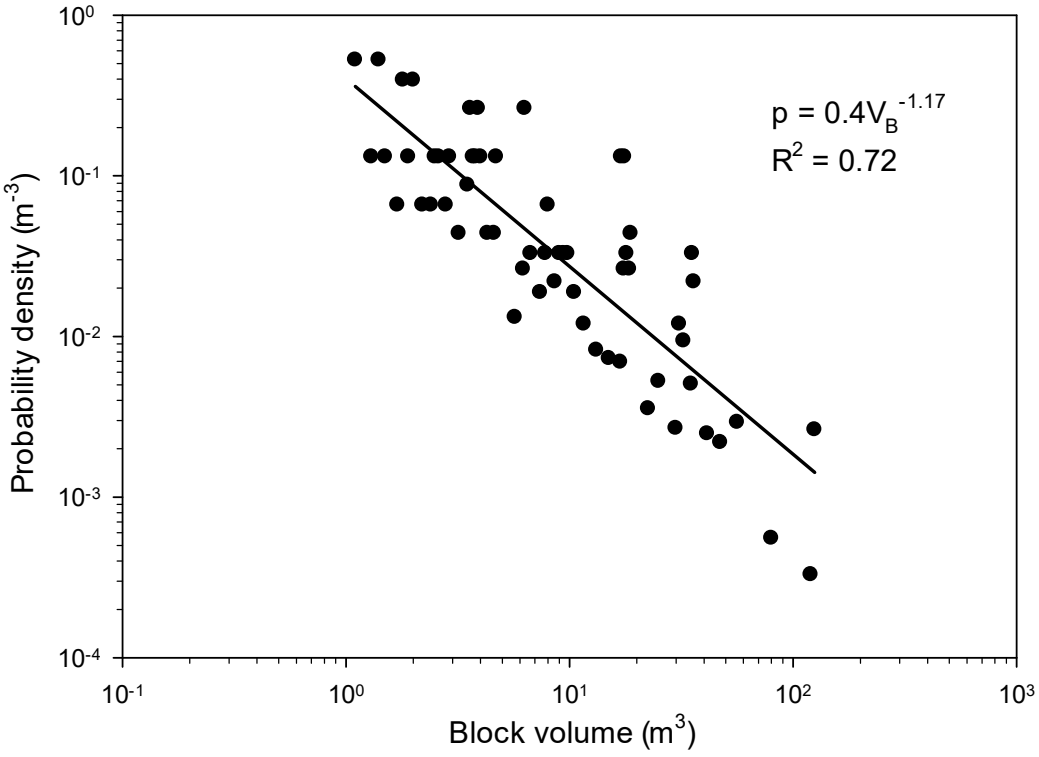
p = 0.4V_B^-1.17
R^2 = 0.72
Probability density (m^-3)
Block volume (m^3)
10^0
10^-1
10^-2
10^-3
10^-4
10^1
10^2
10^3

5 Fig. 6

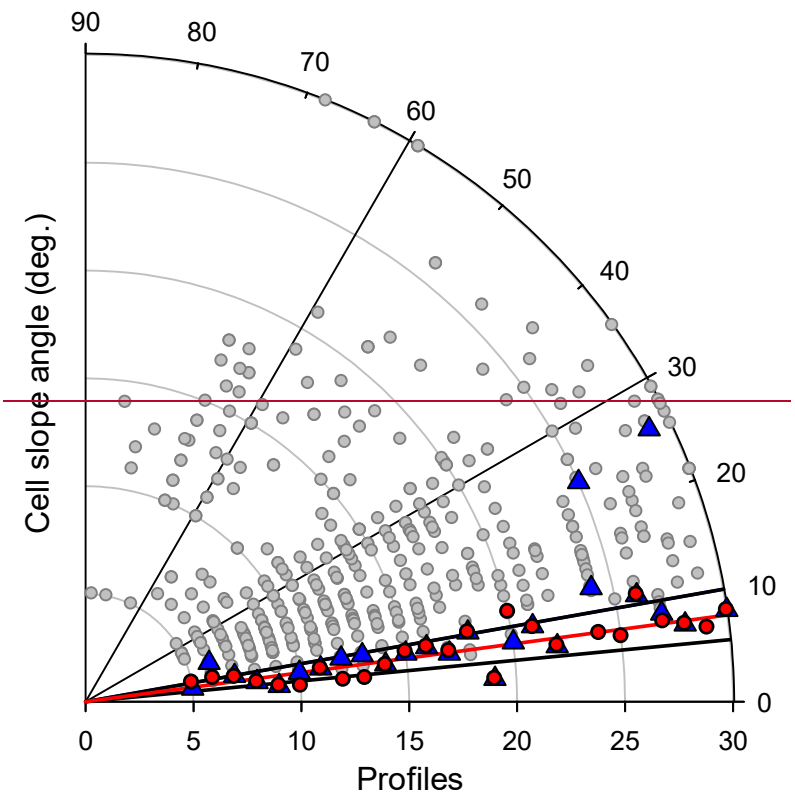
90
80
70
60
50
40
30
20
10
0
Cell slope angle (deg.)
0
5
10
15
20
25
30
Profiles

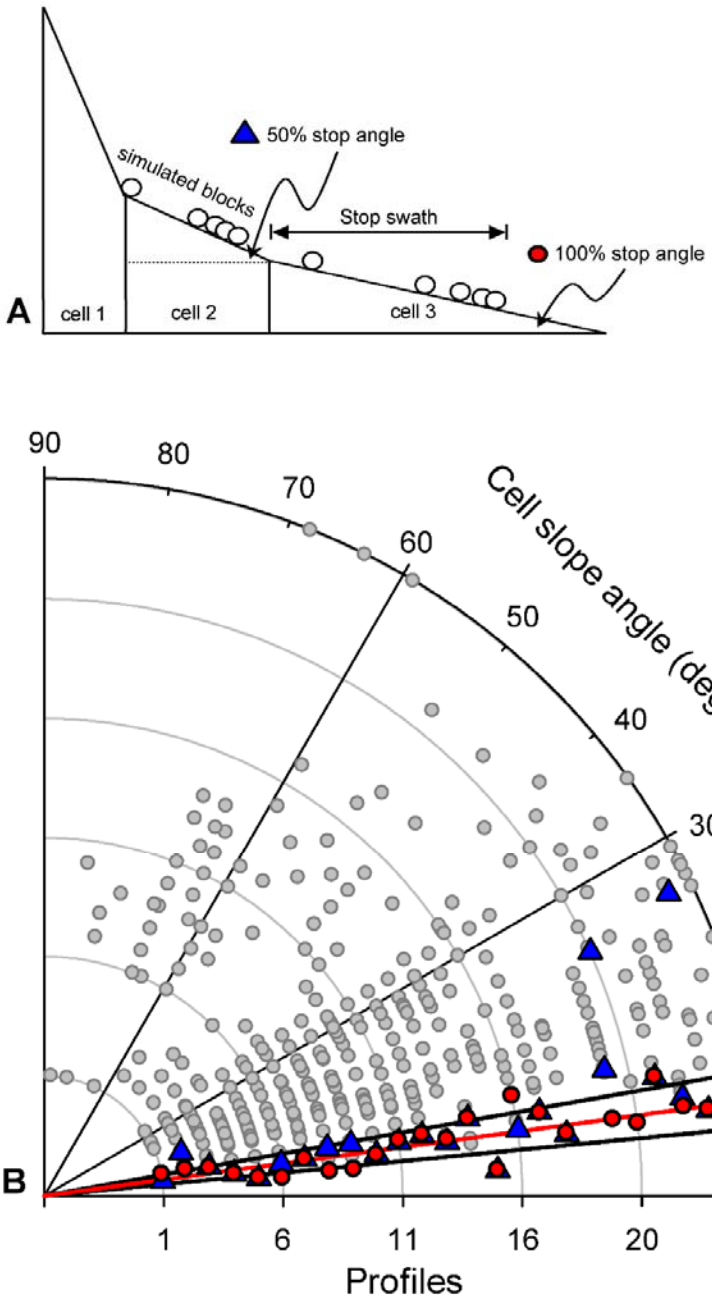
A
cell 1
cell 2
cell 3
simulated blocks
50% stop angle
Stop swath
100% stop angle
B
90
80
70
60
50
40
30
20
10
0
Cell slope angle (deg.)
1
6
11
16
20
25
Profiles

Fig. 7

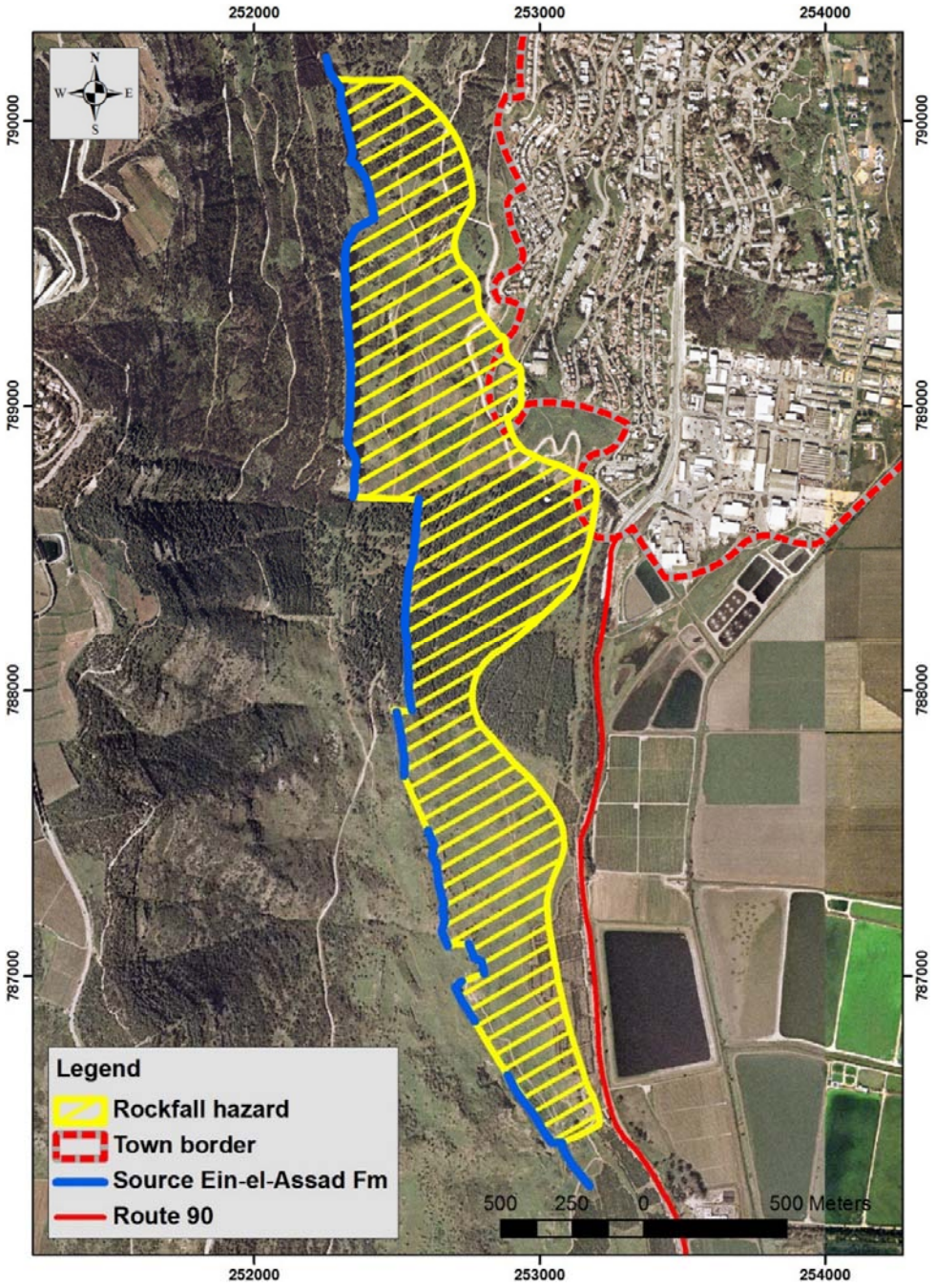
252000
253000
254000
790000
789000
788000
787000
N
W
E
S
Legend
Rockfall hazard
Town border
Source Ein-el-Assad Fm
Route 90
500 250 0 500 Meters

Fig. 8

5

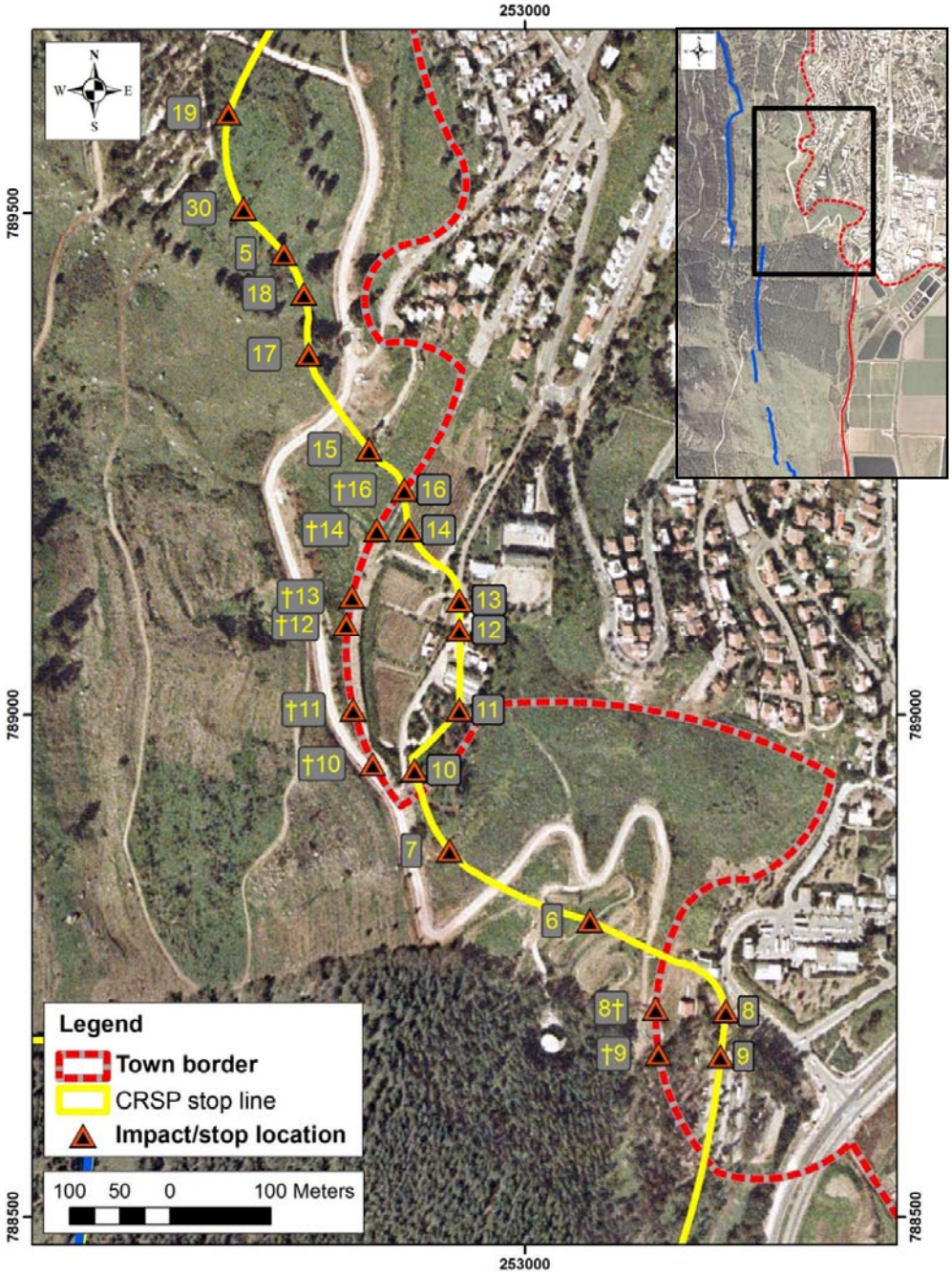
253000
789500
789000
788500
N
W
E
S
19
30
5
18
17
15
†16
16
†14
14
†13
13
†12
12
†11
11
†10
10
7
6
8†
8
†9
9
Legend
Town border
CRSP stop line
Impact/stop location
100 50 0 100 Meters

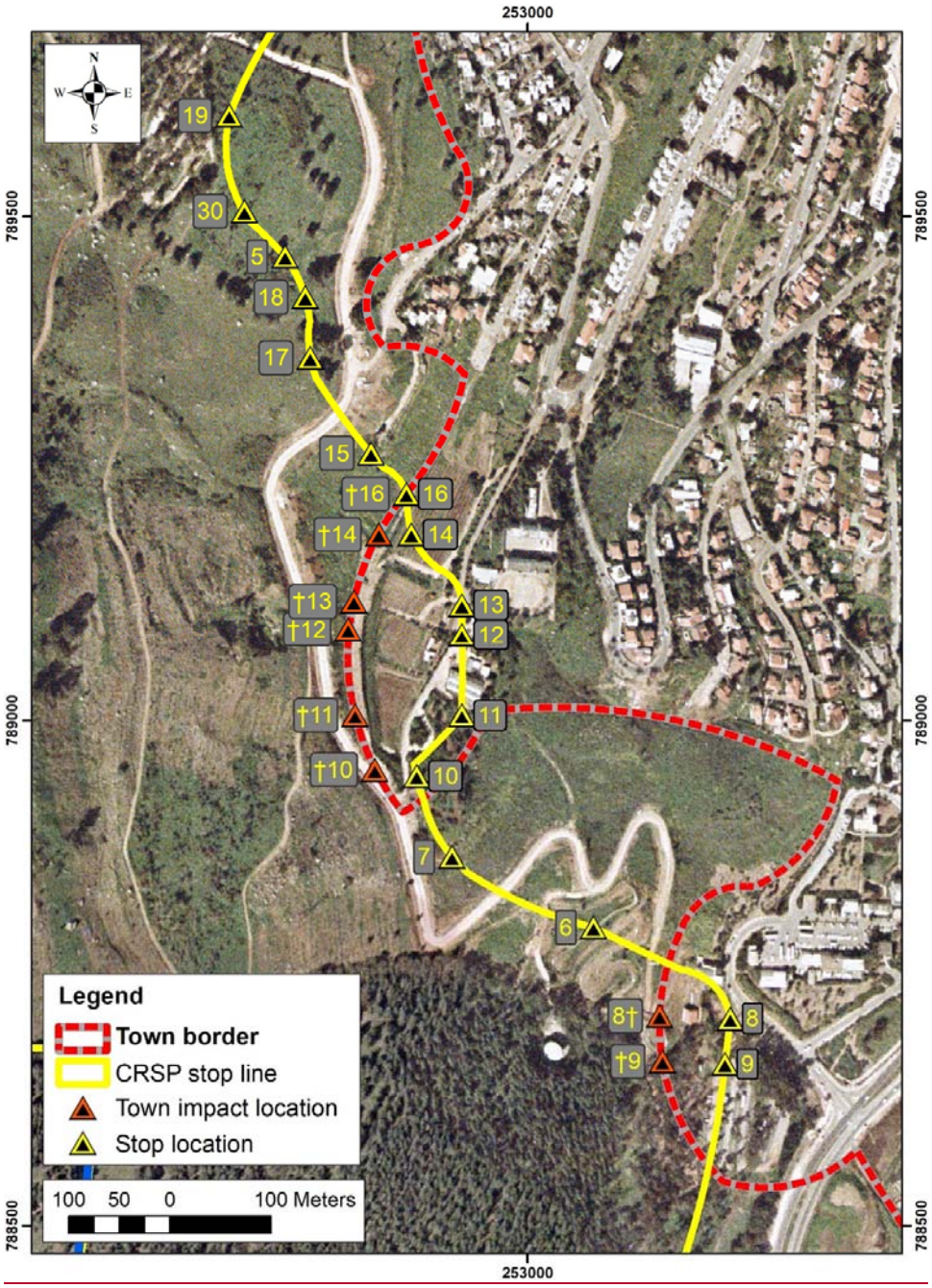
253000
789500
789000
788500
N
W
E
S
19
30
5
18
17
15
†16
16
†14
14
†13
13
†12
12
†11
11
†10
10
7
6
8†
8
†9
9
Legend
Town border
CRSP stop line
Town impact location
Stop location
100 50 0 100 Meters

Fig. 9

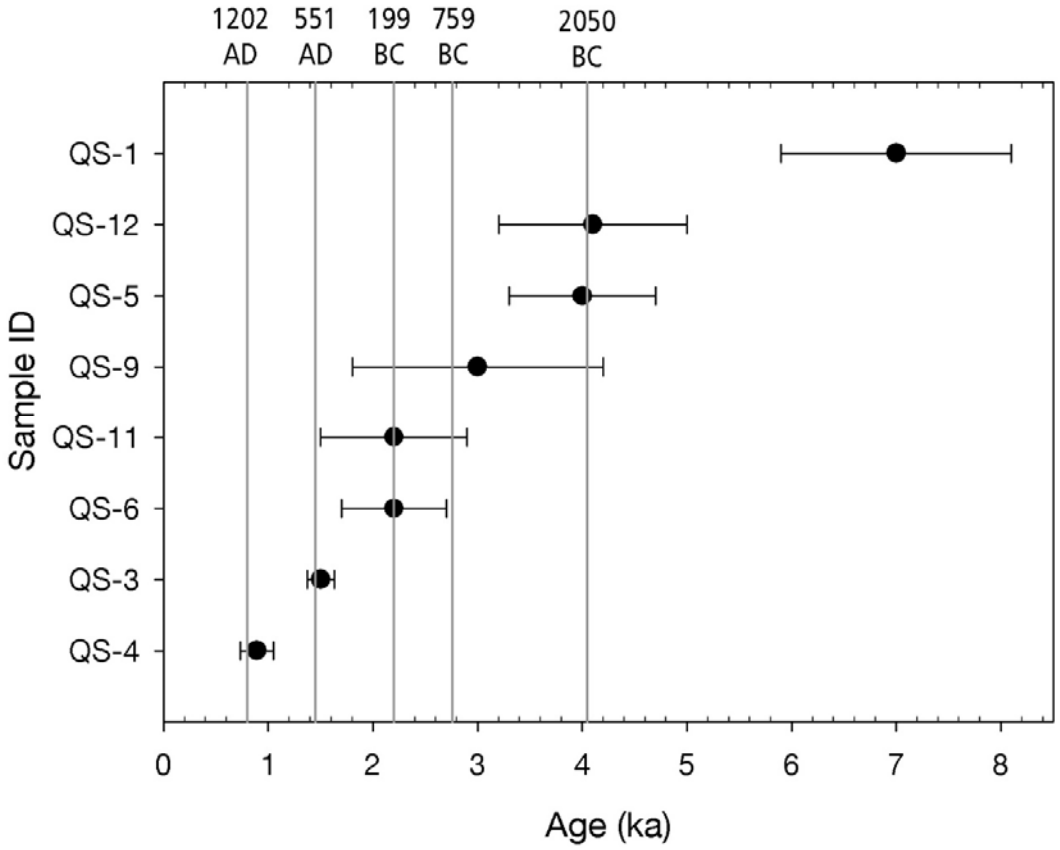
1202 AD
551 AD
199 BC
759 BC
2050 BC
QS-1
QS-12
QS-5
QS-9
QS-11
QS-6
QS-3
QS-4
Sample ID
0
1
2
3
4
5
6
7
8
Age (ka)

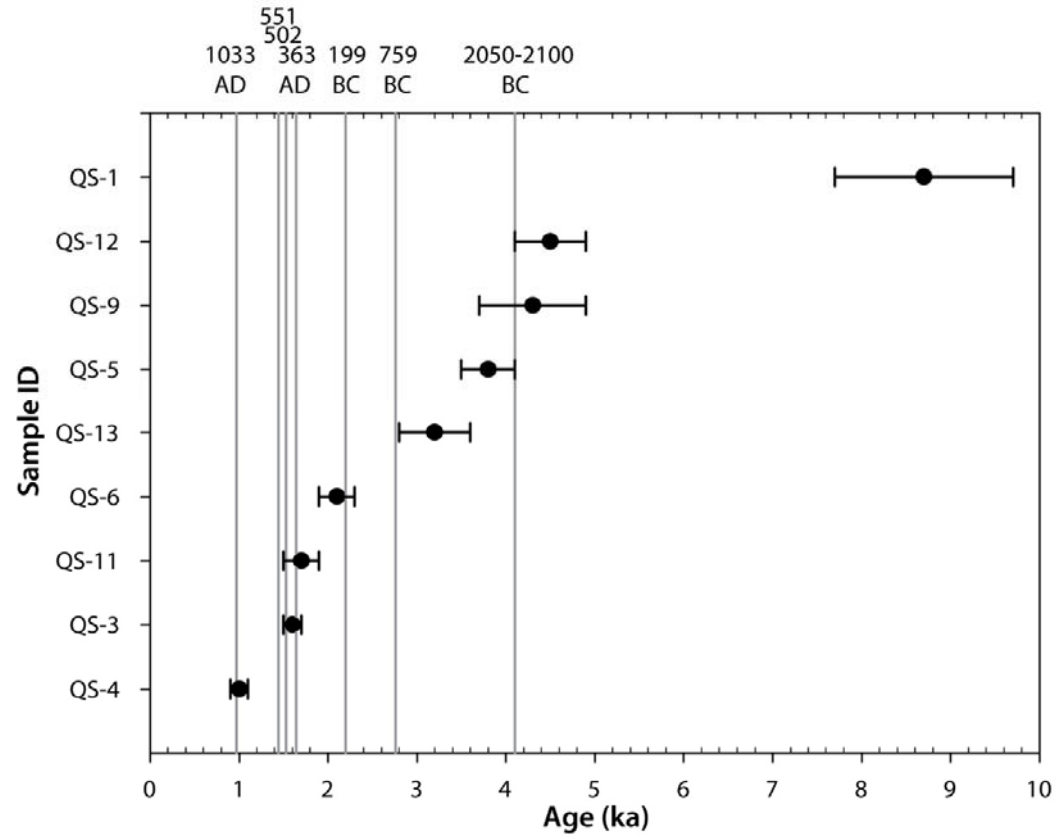
551
502
1033 AD
363 AD
199 BC
759 BC
2050-2100 BC
QS-1
QS-12
QS-9
QS-5
QS-13
QS-6
QS-11
QS-3
QS-4
Sample ID
0
1
2
3
4
5
6
7
8
9
10
Age (ka)

Fig. 10

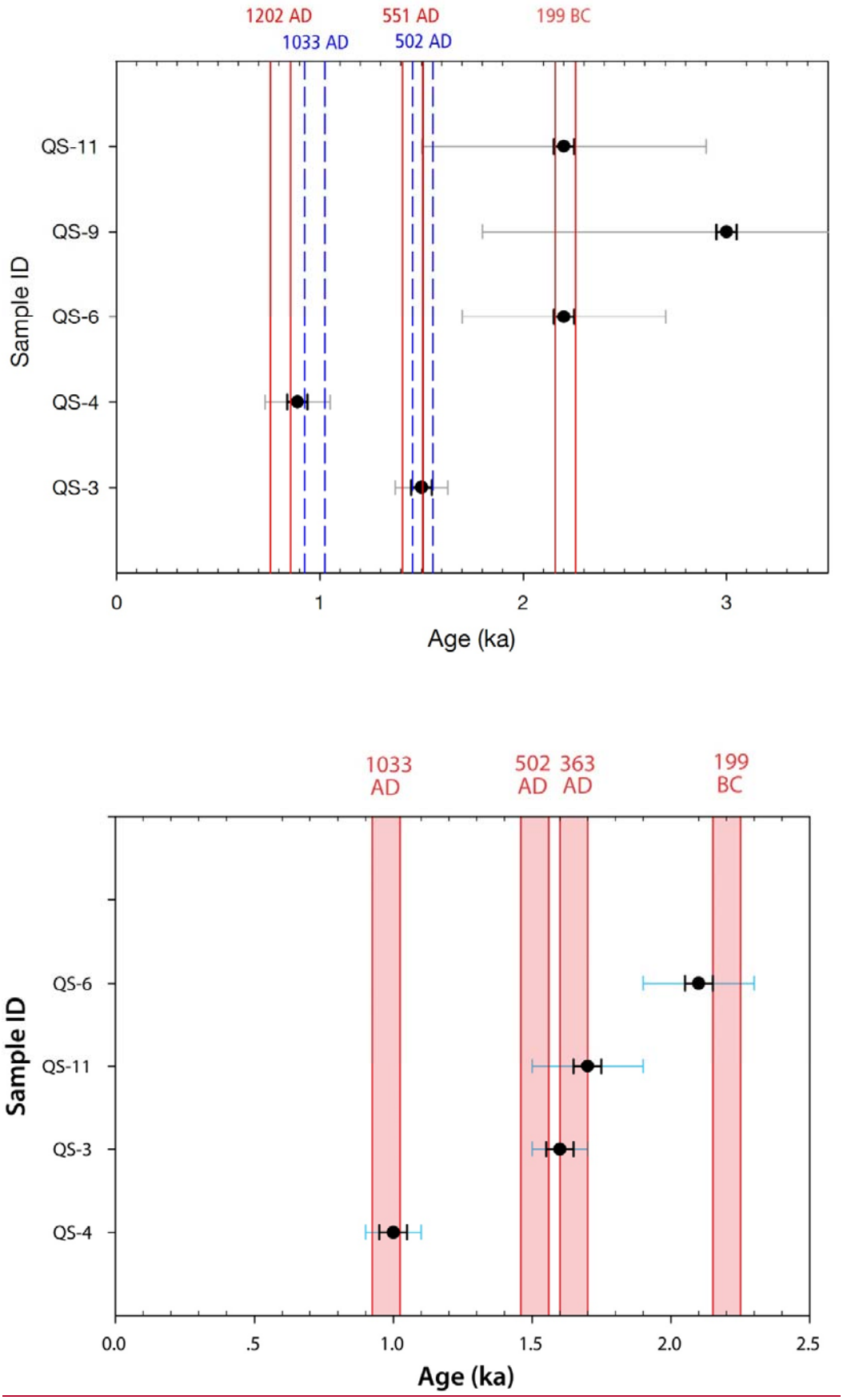
1202 AD
1033 AD
551 AD
502 AD
199 BC
Sample ID
QS-11
QS-9
QS-6
QS-4
QS-3
0
1
2
3
Age (ka)
1033 AD
502 AD
363 AD
199 BC
Sample ID
QS-6
QS-11
QS-3
QS-4
0.0
.5
1.0
1.5
2.0
2.5
Age (ka)

Fig. 11